

Ambient noise levels, Q_{Lg} wave tomography and earthquake source parameters in Norway

Andrea Demuth

Thesis for the Degree of Philosophiae Doctor (PhD)
University of Bergen, Norway
2019

UNIVERSITY OF BERGEN



Ambient noise levels, Q_{Lg} wave tomography and earthquake source parameters in Norway

Andrea Demuth



Thesis for the Degree of Philosophiae Doctor (PhD)
at the University of Bergen

Date of defence: 05.04.2019

© Copyright Andrea Demuth

The material in this publication is covered by the provisions of the Copyright Act.

Year: 2019

Title: Ambient noise levels, Q_{Lg} wave tomography and earthquake source parameters in Norway

Name: Andrea Demuth

Print: Skipnes Kommunikasjon / University of Bergen

**Ambient noise levels,
 Q_{Lg} wave tomography and earthquake
source parameters in Norway**

Andrea Demuth

Dissertation for the degree philosophiae doctor (PhD)
at the University of Bergen



Department of Earth Science
University of Bergen
Norway

21st December 2018

Preface

This thesis was submitted to the Earth Science Department of the University of Bergen for approval of the degree Philosophiae Doctor (PhD). The presented work was carried out at the University of Bergen under the supervision of Prof. Lars Ottemöller and co-supervision of Assoc. Prof. Henk Keers and Prof. Kuvvet Atakan.

The work started in September 2013 with my enrolment to the PhD program of the University of Bergen. I was funded by the Norwegian National Seismic Network project, which is financially supported from the Norwegian Oil and Gas Association.

The structure of the thesis is article-based and divided into two parts. The first part provides an overview of the seismicity in Norway, the research questions, the applied methods and the results. This is followed by the main outcome of this thesis, three scientific papers. Two papers are published in peer-reviewed journals and one is submitted.

Andrea Demuth

21st December 2018

Acknowledgement

Firstly, I like to thank my supervisors Lars Ottemöller, Henk Keers and Kuvvet Atakan for their permanent guidance and support. Lars Ottemöller helped me develop my personality, strengthen my scientific work and my writing skills. I am extremely grateful for your support and the time you invested in me. Henk Keers, I would like to thank you, for your open door, your advice, your personal interest and for your inspiring mathematical passion.

During my time at the Department of Earth Science, my co-workers and the administrative staff have always been helpful and supportive. I'm very grateful for that. In particular, I would like to express my sincere gratitude to Gunn Mangerud and Terje Erstad, who supported and encouraged me to continue with my thesis. Thank you for giving me the chance to prove myself.

A special thanks goes to my co-workers and friends Kathrin Spieker and Karin Landschulze. Thank you for all the enlightening conversations, for your advice and your support. I enjoyed the time with you a lot and feel grateful for it.

I thank my dear friend Francesca Bonetti for a final grammar check and many stimulating conversations.

I would like to express my deepest appreciation to my parents. They encouraged and inspired me my whole life and supported me with their wisdom and friendship. I know, I can always count on you and for that feeling I'm sincerely grateful.

I cannot begin to express my thanks to my husband, who had the patience and strength to stay by my side during this time. He not only supported my academic goals, but also helped to turn my life long dream of a family into reality. Thank you!

Abstract

Norway is part of an intraplate environment and therefore experiences low to intermediate seismicity. This seismicity is a response to the stress field in the lithosphere, which is mainly influenced by ridge push from the Mid-Atlantic ridge. In order to analyse the seismicity in Norway, this thesis first quantifies the ambient seismic noise levels and the detection capability of the Norwegian National Seismic Network (NNSN). Following, it assesses Lg wave attenuation and estimates earthquake source parameters.

The recordings of the NNSN in 2013 are analysed in terms of ambient seismic noise levels. A local noise model for Norway is derived, and geographic and temporal variations are assessed. The sources of ambient seismic noise have specific frequency bands, such as the microseismic peak (4-8 s), which relates to oceanic waves. This thesis obtains a correlation between the microseismic peak and wave heights up to 900 km offshore. Furthermore, a correlation between human activity, especially in the bigger cities, and daily noise level variations is observed. In particular, those noise level variations are used to quantify the station and network performance in Norway. The network capability to detect local and regional events decreases by 0.5 units of magnitude if high frequency noise generated by human activity increases by 10 dB. This observation is incorporated into the presented detection threshold map of Norway.

In order to assess Lg wave propagation, this thesis analyses attenuation of Lg waves using 1369 observations from 279 earthquakes recorded between 1990 and 2017. Initially, Lg wave propagation is quantified through Lg/Pn amplitude ratios. High Lg/Pn ratios, as obtained for onshore regions, imply efficient Lg wave propagation. Offshore regions show mainly inefficient Lg propagation. In order to study this in more detail, Lg wave attenuation was calculated. The calculation obtains an average attenuation of $Q_{Lg}(f) = 529f^{0.42}$ for mainland Norway. Using a tomographic inversion approach, three tomographic maps are presented. These show Lg wave attenuation at 2 Hz, 4 Hz and 6 Hz. The maps reveal significant variations between on- and offshore regions, with higher attenuation offshore. Changes in crustal structure and unconsolidated sed-

iments are thought to be the cause of the relatively high Lg wave attenuation. Finally, this thesis presents estimated earthquake source parameters from events located in Norway and the Svalbard archipelago. The earthquake source parameters are derived using the empirical Green's function method. Between January 1990 and May 2018, the database of the NNSN contains 263 earthquake pairs to which the method was applied. The corresponding 107 master events have a local magnitude range of 1.3-3.4. Assuming a Brune source model, stress drops between 0.4 bar and 355 bar are obtained. We observe increasing stress drop with increasing seismic moment, which contradicts earthquake self-similarity.

List of publications and authorship statement

The main part of the thesis, which consists of three articles, evolved through collaborative work. I am the first author of all three papers and my contribution to these papers is listed below.

1. **Ambient seismic noise levels and detection threshold in Norway**

Andrea Demuth, Lars Ottemöller, and Henk Keers

Journal of Seismology (2016) 20, 889-904 (published)

I processed the data, generated the figures and wrote the manuscript. My co-authors discussed with me the work and reviewed the manuscript. I did 85 % of the work.

2. **Q_{Lg} wave tomography beneath Norway**

Andrea Demuth, Lars Ottemöller, and Henk Keers

Journal of Seismology (2018) (published)

I developed the code to perform the tomographic inversion, processed the data, generated the figures and wrote the manuscript. My co-authors discussed with me the work, pointed out bugs in the program and reviewed the manuscript. I did 85 % of the work.

3. **Earthquake source parameters in Norway determined with empirical Green's functions**

Andrea Demuth, Norunn Tjøland, and Lars Ottemöller

(submitted to Journal of Seismology)

I processed the data, generated the figures and wrote the manuscript. My co-authors discussed with me the work and reviewed the manuscript. I did 85 % of the work.

Contents

Preface	i
Acknowledgement	ii
Abstract	iii
List of publications and authorship statement	v
1 Introduction	3
2 Theory and methods	7
2.1 Seismic source model	8
2.2 Attenuation	11
2.3 Q_{Lg} tomography	12
2.4 Seismic noise	14
3 Results	15
3.1 Ambient seismic noise and detection threshold	15
3.2 Q_{Lg} wave tomography	17
3.3 Earthquake Source Parameters	20
4 Conclusion	23
5 Publications	25
5.1 Paper 1: Ambient noise levels and detection threshold in Norway	25
5.2 Paper 2: Q_{Lg} wave tomography beneath Norway	47
5.3 Paper 3: Earthquake Source Parameters in Norway determined with Empirical Green's functions	63
Errata	77
References	79

1 Introduction

Norway lies in an intraplate environment and is topographically dominated by the southwest-northeast elongated Caledonian mountain range (Fig. 1). Offshore mid-Norway a passive continental margin forms the transition zone from continental to oceanic crust. Towards the south, the passive continental margin extends into the North Sea Basin which has several graben structures.

Besides deglaciation and local sediment loading, the stress field in Norway is mainly influenced by ridge push from the Mid-Atlantic ridge (Bungum et al., 2010). The ridge push causes stress to accumulate. This often results in brittle failure of rocks and thus earthquakes.

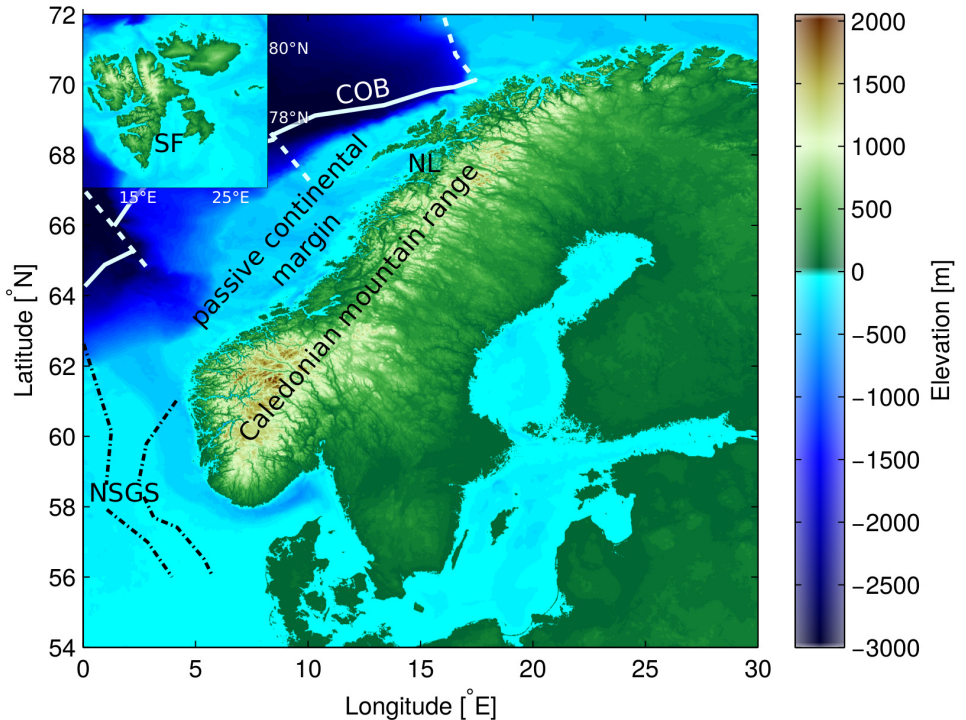


Figure 1: Topographic map of Norway and the Svalbard archipelago (upper left corner). Basic geological structures and areas referred to in the text are sketched on top: the North Sea graben system (NSGS), Nordland (NL), the continental-oceanic boundary (COB) and Storfjorden (SF) in Svalbard.

Norway experiences low to intermediate seismicity (Fig. 2). Most earthquakes occur along the graben system of the northern North Sea, the edge of the passive continental margin off mid-Norway and the coastline, especially in south-western Norway and northern Norway (Nordland). Bungum et al. (1982), Atakan et al. (1994) and Hicks et al. (2000) studied earthquake sequences in Nordland in more detail and observed swarm-like characteristics. Locally increased seismic activity is also observed in Storfjorden, Svalbard (Pirli et al., 2010).

Seismicity in Norway is recorded by the Norwegian National Seismic Network (NNSN), which was established in 1992. Today, the network consists of 34 stations. Around 3500 earthquakes are recorded by the NNSN every year, most of them have local magnitude less than 5.

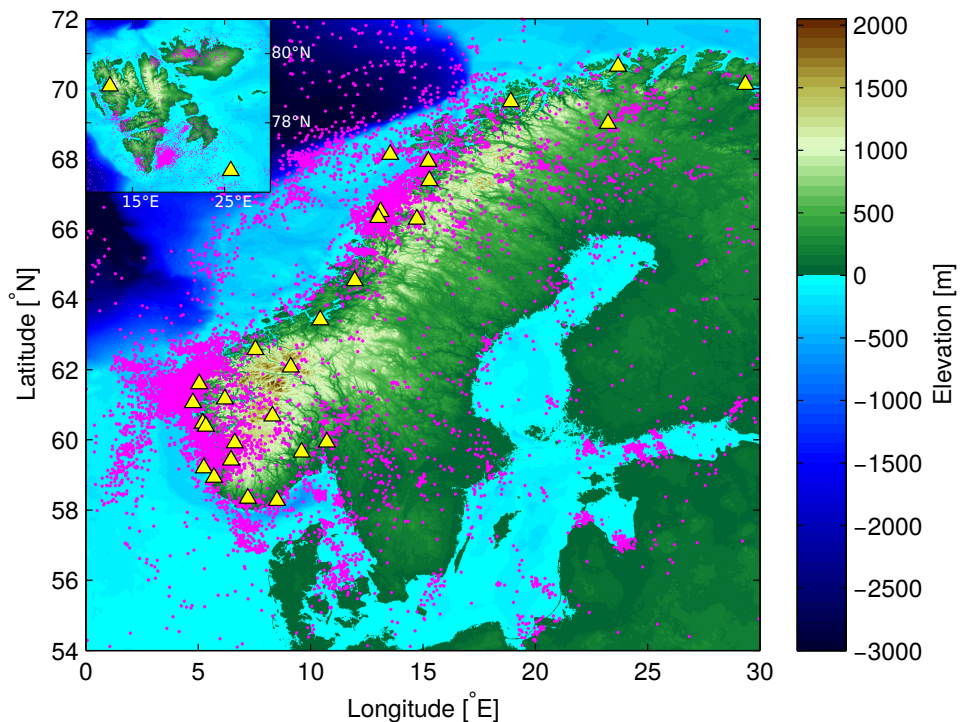


Figure 2: Earthquakes (pink dots) recorded by the NNSN between January 1990 and Mai 2018 for Norway and Svalbard (upper left corner). Yellow triangles indicate stations of the NNSN.

The capability of a network to detect an earthquake depends on the station distribution, seismic equipment, vault construction and noise levels at each station. Ambient seismic noise is generated by multiple sources in specific frequency bands, e.g. human activity (1-20 Hz) and oceanic waves (4-16 s). Peterson (1993) developed an approach to quantify ambient seismic noise. This was later extended by McNamara & Buland (2004) who computed probabilities of noise occurrence. Based on the noise levels, the temporal and spatial variations in detection thresholds of networks are assessed (e.g. Marzorati & Bindi, 2006).

Monitoring of seismic activity in Norway is crucial to gain a better understanding of current seismotectonics. In order to analyse and interpret seismic data, a solid knowledge of wave propagation across Norway is needed. In particular, this concerns knowledge of variations in velocities and attenuation. The attenuation depends on intrinsic absorption and scattering, thus on local geology. Lg wave propagation is often used in attenuation studies (e.g. Campillo & Plantet, 1991; Benz et al., 1997; Ottemöller et al., 2002). Generally, tectonic active areas, regions with partial crustal melting, very thin continental crust, oceanic crust and deep sedimentary basins attenuate Lg waves more than older tectonically stable areas such as shields and cratons (e.g. Singh & Herrmann, 1983; Gregersen, 1984; Kennett & Mykkeltveit, 1984; Zhang & Lay, 1995; Fan & Lay, 2002).

The source signal, or source time function of an earthquake, is described by earthquake source parameters such as rupture time, source radius, seismic moment and stress drop. The most controversial parameter is the stress drop. In theory, the correlation between stress drop and seismic moment reveals fundamental characteristics of earthquakes. For example, studies by Aki (1967), Prieto et al. (2004) and Abercrombie et al. (2017) obtained a constant stress drop over all magnitude ranges and therefore suggest earthquake self-similarity. Earthquake self-similarity implies the same faulting slip to fault dimension ratio for small and large earthquakes. However, Hasegawa (1983), Mori et al. (2003) and Malagnini et al. (2014), among others, observed a break down of self-similarity for small magnitudes (< 3).

Starting from these considerations, the goal of this thesis is to improve the understanding of seismicity in Norway. First, the geographical and temporal variations of ambient seismic noise levels are quantified, in order to evaluate the network performance, detection threshold and data quality of individual stations. The second paper of this thesis aims to map attenuation variations in Norway and to correlate them with geological structures. The knowledge of Lg wave attenuation decreases uncertainties in spectral analysis of earthquakes and therefore improves, for example, seismic hazard assessments. In the third paper of this thesis, earthquake source parameters in Norway are estimated and their regional variations are analysed as well as the self-similarity of events.

2 Theory and methods

The Earth is in permanent vibration due to oceanic waves, changes in the atmosphere and human activity. In seismic ground motion recordings, those low amplitude vibrations are named seismic noise. Higher amplitude motions are generated by seismic sources of natural origin (e.g. earthquakes, volcanic tremor, landslides) or man-made (e.g. explosions).

The seismic signal generated at the source propagates through the Earth and interacts with its internal structure. Thus, the recorded seismic signal contains information about the seismic source as well as the structure along the propagation path. Therefore, the signal is influenced by the source, geometrical spreading, attenuation, and the receiver site effects. The instrument corrected amplitude spectrum $A(f)$ of an earthquake can be written as

$$A(f) = S(f) L(f) H(f) G(R) \quad (1)$$

where, the source term at frequency f is denoted by $S(f)$, the site term by $L(f)$, attenuation by $H(f)$ and geometrical spreading by $G(R)$. Following Herrmann & Kijko (1983) the geometrical spreading is

$$G(R) = \begin{cases} R^{-1} & R < R_x \\ (R_x R)^{-1/2} & R > R_x \end{cases} \quad (2)$$

where the epicenter distance is R and R_x is twice the crustal thickness. These equations assume a dominance of body waves when $R < R_x$ and a dominance of surface waves when $R > R_x$. More details on source signal and attenuation are provided in the following subsections. The last two subsection give an overview on tomographic inversion and calculation of ambient seismic noise.

2.1 Seismic source model

The source time function (Fig. 3a) of an earthquake depends on the faulting area, the rigidity of the rock, the slip length and rupture velocity. These source parameters describe the physical characteristics of an earthquake. The integral over the source time function provides a measurement of earthquake size, the seismic moment (M_0 [Nm]) (Boatwright, 1980). Kanamori (1977) used the seismic moment to define the moment magnitude

$$M_w = \frac{2}{3} \log_{10}(M_0) - 6.07 \quad (3)$$

Transferring the source time function into frequency domain, Brune (1970) describes the source spectrum as

$$S(f) = \frac{\Omega_0}{1 + \left(\frac{f}{f_c}\right)^2} \quad (4)$$

with a long-period plateau value Ω_0 (relative seismic moment) and a ω^2 fall-off for frequencies (f) larger than the corner frequency f_c . An alternative source model with a steeper fall-off of ω^3 was proposed by Boatwright (1980). The difference between both models is shown in Figure 3b.

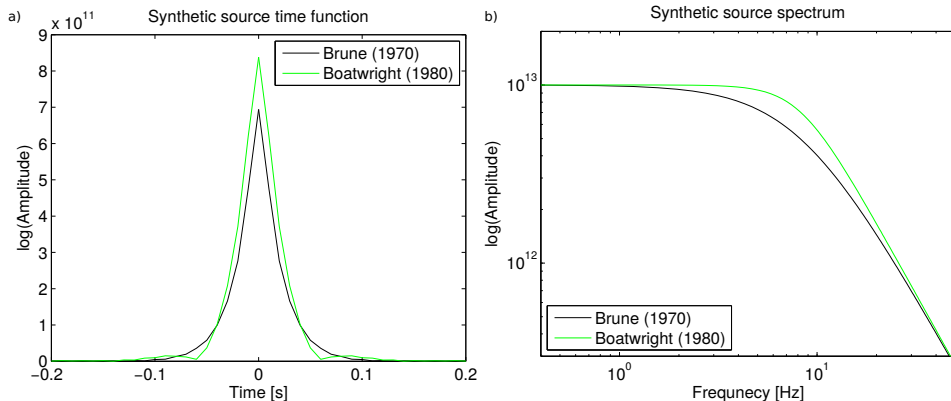


Figure 3: a) Synthetic source time function calculated after Brune (1970) (black) and Boatwright (1980) (green) corresponding to a seismic moment of 10^{13} Nm. b) Theoretical source spectrum with a seismic moment of 10^{13} Nm.

The two source models of Brune (1970) and Boatwright (1980) are commonly used and assume a circular fault. However, they differ in the fall-off rate as well as in the way the source radius of an earthquake is estimated. Assuming an instantaneously rupturing fault, Brune (1970) proposed a source radius r_0 given by

$$r_0 = 0.35 \frac{\beta}{f_c} \quad (5)$$

which is thus proportional to the ratio of S-wave velocity at the source (β) and corner frequency (f_c). Real faults behave more complicated. The rupture begins and propagates along the fault with a rupture velocity v_r . The amount of time needed for the propagation process is termed rupture time τ and corresponds to the width of the source time function. The recorded signal at a station varies not only with rupture time, but also with its azimuth θ to the initial point of rupture. These additional aspects are incorporated in the estimation of the source radius after Boatwright (1980)

$$r_0 = \frac{\tau_{1/2} v_r}{(1 - v_r \sin \theta / \beta)}. \quad (6)$$

The pulse rise time $\tau_{1/2}$ is approximated as half the rupture time and can be correlated with the corner frequency of the source spectra ($f_c = 1/\pi\tau_{1/2}$). The source radius is very useful as it is used to estimate the stress drop (Eshelby, 1957)

$$\Delta\sigma = \frac{7}{16} \frac{M_0}{r_0^3} \quad (7)$$

In order to isolate the source spectrum of an earthquake from the seismic signal, the signal needs to be corrected for attenuation and path effects (see Eq. 1). In spectral analysis, the attenuation correction is based on an average value and therefore accounts not for individual path conditions. Thus, this approach introduces assumptions and therefore sources of errors. For example, S-waves propagating through oceanic crust experience generally higher attenuation than the ones propagating through continental crust (Zhang & Lay, 1995; McNamara & Walter, 2001). Another problem poses near

surface attenuation at the individual recording sites. Strong near surface attenuation functions as high frequency cut-off and leads to underestimated corner frequencies.

Another approach to obtain earthquake source parameters, the empirical Green's function method, was proposed by Hartzell (1978) and Mueller (1985). This method is based on the assumption that co-located events generated by the same source travel along the same path to the recording station and therefore experience the same path effects. If the events differ in more than one order of magnitude in size, the source time function (STF) of the smaller event can be used as Green's function. The deconvolution of the smaller event (EGF) from the larger one (master event) results in the STF of the master event. The width of the master STF provides the rupture time, which is used to calculate corner frequency, source radius, and therefore stress drop.

2.2 Attenuation

The seismic pulse generated at a source propagates through the Earth and attenuates along the ray path. In Equation (1), attenuation is accounted for by an exponential spectral decay corresponding to

$$H(f) = \exp\left(\frac{-\pi f R}{Qv}\right) \quad (8)$$

where f is the frequency, R the hypocenter distance, Q the quality factor and v the group velocity. Aki (1980) described the frequency dependence of the S-wave quality factor by the power-law relation

$$Q(f) = Q_0 f^\eta \quad (9)$$

where Q_0 is the reference quality factor at a frequency of 1 Hz and η is the constant determining the strength of frequency dependence. In order to derive a power-law relation for Lg waves in Norway, the data was inverted for an average quality factor following the approach of Ottemöller et al. (2002). With the requirement that the hypocenter distance is larger than twice the crustal thickness, Equations (1), (2) and (8) can be combined to give

$$A(f) = S(f) L(f) \exp(-\pi f R / Qv) (R_x R)^{-1/2} \quad (10)$$

Taking the logarithm of Equation (10),

$$\log A(f) + 0.5 \log(R_x R) = \log S(f) + \log L(f) - (\pi f R \log(e)/v) Q^{-1} \quad (11)$$

gives an Equation that is linear in Q^{-1} . If we have kl observations from k earthquakes recorded at l stations then this results in a linear system of equations:

$$\begin{bmatrix} \log A_1(f) + 0.5 \log(R_x R_{11}) \\ \vdots \\ \log A_{kl}(f) + 0.5 \log(R_x R_{kl}) \end{bmatrix} = \begin{bmatrix} 1 & \dots & 0 & 1 & \dots & 0 & \frac{-\pi f \log(e) R_{11}}{v} \\ \vdots & \ddots & \vdots & \vdots & \ddots & \vdots & \vdots \\ 0 & \dots & 1 & 0 & \dots & 1 & \frac{-\pi f \log(e) R_{kl}}{v} \end{bmatrix} \cdot \begin{bmatrix} \log S_1 \\ \vdots \\ \log S_k \\ \log L_1 \\ \vdots \\ \log L_l \\ Q^{-1} \end{bmatrix}. \quad (12)$$

Equation (12) in matrix form is

$$\mathbf{d} = \mathbf{G}\hat{\mathbf{m}} \quad (13)$$

with data vector \mathbf{d} , kernel matrix \mathbf{G} and model vector $\hat{\mathbf{m}}$.

2.3 Q_{Lg} tomography

In order to derive a tomographic image, rather than an average attenuation value, the research area needs to be subdivided into grid cells. The tomographic approach obtains an attenuation value for each grid cell and Equation (11) changes to

$$\log A(f) + 0.5 \log(R_x R) = \log S(f) + \log L(f) - (\pi f R_i \log(e)/v) Q_i^{-1} \quad (14)$$

where R_i is the ray path length crossing through grid cell i with a quality factor Q_i . Equation (14) poses a linear inverse problem. Following Ottemöller et al. (2002), who applied the method of Barmin et al. (2001), the model vector can be solved as

$$\hat{\mathbf{m}} = \tilde{\mathbf{G}}\mathbf{d} \quad (15)$$

with the computed generalized inverse matrix

$$\tilde{\mathbf{G}} = (\mathbf{G}^T \mathbf{G} + \mathbf{P})^{-1} \mathbf{G}^T. \quad (16)$$

The regularization matrix

$$\mathbf{P} = \mathbf{F}^T \mathbf{F} + \mathbf{K}^T \mathbf{K} \quad (17)$$

stabilises the mixed determined problem with a smoothing (\mathbf{F}) and damping (\mathbf{K}) constraint. The components of the smoothing matrix is given as

$$F_{ij} = \begin{cases} \alpha & i = j \\ \alpha V_{ij}/p_j & i \neq j \end{cases} \quad (18)$$

with

$$V_{ij} = \exp(-R_{ij}^2/2\sigma^2) \quad (19)$$

and

$$p_j = \sum_{i=1, i \neq j}^Y V_{ij}. \quad (20)$$

α is the smoothing constant, σ the smoothing width and R_{ij} represents the distance between grid cell i and j . The damping matrix

$$K_{ij} = \begin{cases} 0 & i \neq j \\ \beta \exp(-\lambda L_i) & i = j \end{cases} \quad (21)$$

applies the damping parameter β dependent on the sum of all travel path segments L_i crossing grid cell i .

2.4 Seismic noise

Random low amplitude vibrations in seismograms, also known as ambient seismic noise, are used as continuously recorded signal and can be analysed, for example, in terms of its power spectral amplitude. Peterson (1993) developed a global noise model and established a common method to evaluate seismic noise levels.

The standard approach to analyse seismic background noise is to calculate the power spectral density (PSD)

$$P_k = \frac{2\Delta t}{N} |Y_k|^2, \quad (22)$$

which is proportional to the squared amplitude spectrum (Y_k) at a discrete frequency f_k . The ratio of twice the sampling interval (Δt) and the number of samples (N) provides a normalization factor to correlate the PSD to the global reference model of high and low noise levels derived by Peterson (1993).

McNamara & Buland (2004) proposed the calculation of probability density functions (PDF) to assess statistical variations of PSD over a certain time period. Therefore, the probability of noise at a certain period (T_c) can be calculated as

$$P(T_c) = N_{PT_c}/N_{T_c}. \quad (23)$$

The number of spectral estimates N_{PT_c} is calculated over 1 dB power bins, ranging between -200 dB and -80 dB. The total number of the spectral estimates is given by N_{T_c} .

3 Results

3.1 Ambient seismic noise and detection threshold

Ambient seismic noise levels in Norway are expected to change with cultural activities and seasonal weather conditions. In this subsection the main observations on noise level variations and their influence on the detection threshold of the NNSN are summarised and presented.

Noise levels in the long period range 1-35 s increase during the winter months and correlate with relatively rough weather conditions (Fig. 4). We observe up to 22 dB higher noise levels during the winter in Norway. For comparable periods, a noise level increase during the winter of 25 dB has been reported for northern Italy (Marzorati & Bindi, 2006), 15-20 dB for the US (McNamara & Buland, 2004) and 20 dB for Iberia and Morocco (Díaz et al., 2010). Thus, the high period noise level increase in Norway is similar to the increase observed in other regions. During the summer, long period noise levels are lower, except for a few individual peaks related to storms. Arduin et al. (2012) suggested that long period noise levels can be related to wave heights. We were able to obtain a correlation between long period noise and wave heights up to 900 km offshore.

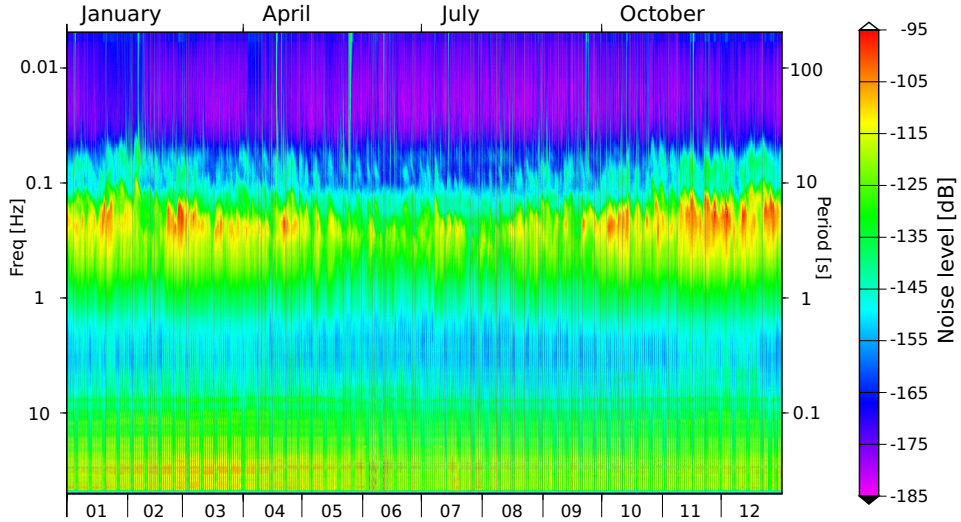


Figure 4: PSD spectrogram calculated for the vertical component of the station in Tromsø 2013.

High frequency noise (> 1 Hz) varies on a daily basis due to human activities. These variations are mainly observed in bigger cities, which show increased noise levels of up to 15 dB. However, most stations of the NNSN experience a variation of less than 5 dB. High frequency noise level variations observed across the US (McNamara & Buland, 2004), northern Italy (Marzorati & Bindi, 2006) and the North Island of New Zealand (Rastin et al., 2012) range between 7 dB and 20 dB. The lower variations in Norway are partly explained by its low population density.

The observed noise levels were used to determine the influence of noise on the detection threshold of the NNSN. An increase of noise by 10 dB decreases the detection threshold of earthquakes by 0.5 units of magnitude. Thus, the high frequency noise level variations observed in bigger cities increases the detection threshold of local and regional events by up to 0.75 units of magnitude. The detection threshold of teleseismic events increases by 0.25 units of magnitude due to seasonal noise level variations. Individual storms can increase the detection threshold even more. For example, in 2013 an increase by up to 1.5 units of magnitude was observed because of such a storm.

Based on the station configuration, we computed synthetic detection thresholds of the NNSN and included increased noise levels in bigger cities in a second model (Fig. 5).

Figure 5 shows the smallest local magnitude observed by the NNSN together with the two synthetically calculated detection threshold maps. The synthetic models compare well with the smallest observed earthquakes and indicate a detection threshold of M_L 1 for mainland Norway and M_L 3 for the Norwegian Sea. Detection thresholds of 1.4, 1.8 and 2-2.5 are found for Alaska (D’Alessandro & Ruppert, 2012), Greece (D’Alessandro et al., 2011b) and Italy (D’Alessandro et al., 2011a), respectively. Hence, the detection threshold obtained for Norway is comparable to other networks. This is, however, just an indication, since station performances and seismic attenuation can significantly effect the result.

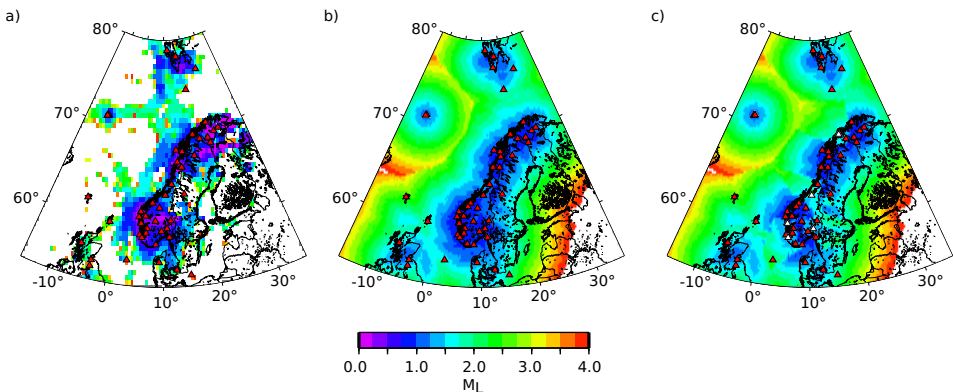


Figure 5: Detection threshold maps of Norway. Triangles provide the position of seismic stations. (a) Smallest local magnitude observed by the NNSN. (b) Theoretical detection threshold of Norway. (c) Theoretical detection threshold of Norway with increased high frequency noise levels in bigger cities (white stations).

3.2 Q_{Lg} wave tomography

Lg waves are dominant on regional records. Due to their sensitivity to lateral crustal changes, Lg wave analysis provides information on the geological structure. First, we quantified Lg wave propagation in terms of their efficiency relative to Pn waves. We then performed an attenuation analysis. The main results are summarised here.

High Lg/Pn amplitude ratios (> 3), corresponding to efficient Lg wave propagation, are obtained for ray paths propagating through mainland Norway. Rays crossing offshore

areas show low Lg/Pn amplitude ratios, thus inefficient Lg wave propagation. To verify this in more detail, a tomographic inversion is performed. First, an average quality factor of $Q_{Lg}(f) = Q_0 f^\eta = 529 f^{0.42}$ was derived for mainland Norway and used as a starting value in Lg wave attenuation tomography. Earlier studies by Kvamme et al. (1995) and Sereno et al. (1988) derived a value of Q_0 for Norway of 440 and 420-570, respectively. These are overall in line with our value. Furthermore, the quality factor derived for Norway corresponds to low Lg wave attenuation, which is typical for an intraplate environment. Low Lg wave attenuation is for example also observed in the north east and central US (Singh & Herrmann, 1983; Erickson et al., 2004).

We performed a checkerboard test to quantify the limitations of our tomographic inversion. The synthetic test (Fig. 6) was performed using the real ray path coverage, the same damping and smoothing parameters as in the tomographic inversion, a grid cell size of 1° by 1° and a box size of 4° by 4° . The test confirmed the ability of the approach and dataset to resolve attenuation variations in mainland Norway and the mid-Norwegian margin on a scale of about 400 km.

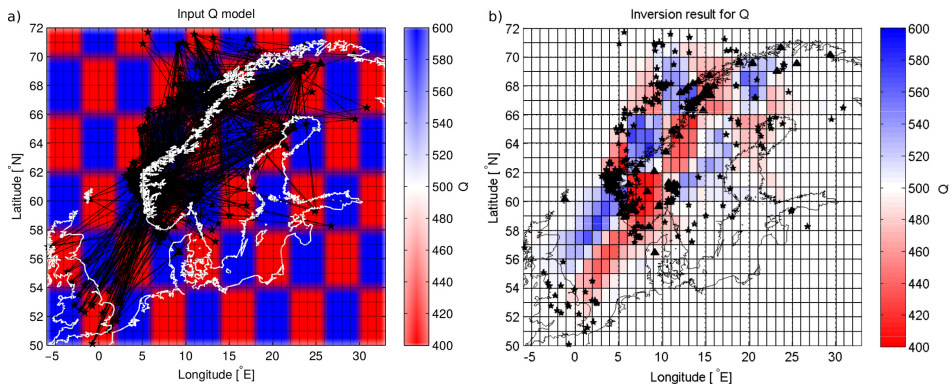


Figure 6: Results of the synthetic inversion checkerboard test. Stations and earthquakes are indicated by triangles and stars, respectively. (a) Input Q model with box size 4° by 4° . The inversion is performed for grid cell sizes of 1° by 1° and results are shown in (b).

The tomographic maps (Fig. 7) reveal a distinct variation in Lg wave attenuation between on- and offshore regions. The mid-Norwegian margin gives rise to higher than average attenuation. Lower than average attenuation is obtained for mainland Norway. Those variations are best resolved at lower frequencies. Zhang & Lay (1995) and Shapiro et al. (1996) used synthetic modelling to show the impact of oceanic-continental transition zones and low velocity surface layers on Lg wave amplitudes. They found strong Lg wave attenuation in the transition zones and Lg wave extinction in soft sediments. We attribute the increased Lg wave attenuation in the mid-Norwegian margin to changes in crustal structure and unconsolidated sediments. Smaller scale variations as indicated by ellipses A-D can also be associated with geological features, but are close to the resolution limits.

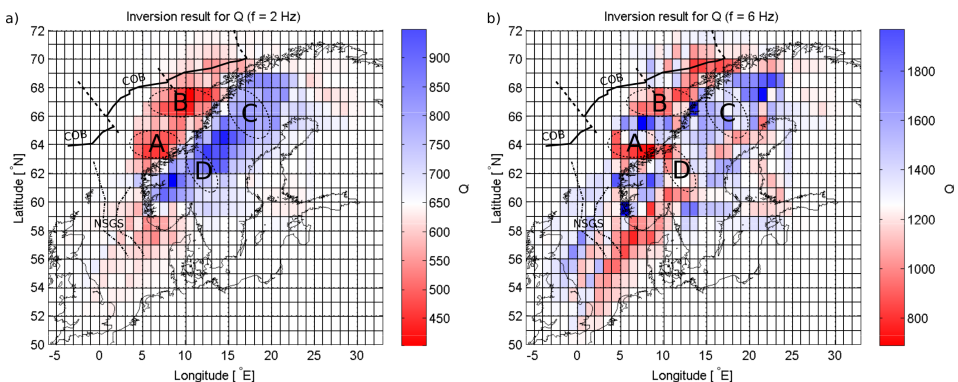


Figure 7: Tomographic maps of Lg wave attenuation at frequencies of (a) 2 Hz and (b) 6 Hz. The color of the background QLg value is set to white. Positive perturbations are indicated with blue and negative ones with red. The ellipses A-D highlight areas of higher attenuation in the mid-Norwegian Margin and mainland Norway. Structural elements are sketched on top: NSGS, North Sea Graben System; COB, continental oceanic boundary.

3.3 Earthquake Source Parameters

The source time function of an earthquake is described with the help of earthquake source parameters. These parameters provide information on the mean fault plane of an earthquake and therefore about their variation over size. This subsection summarises our findings on earthquake source parameters in Norway.

We computed earthquake source parameters for 107 events recorded in Norway and the Svalbard archipelago. Our main focus was on stress drop. Based on the Brune source model and the EGF method, we obtained stress drops between 0.4 bar and 355 bar. The stress drop range appears to be large, but is comparable to stress drops derived, for example, in the northeastern US (Shi et al., 1998). Shi et al. (1998) support the theory that up to a threshold magnitude of 3, the stress drop increases with increasing seismic moment. For larger magnitude values the stress drop is constant. We observe an increase of stress drop with increasing seismic moment for events up to a local magnitude of 3.4 (Fig. 8a). For events larger than that, we are not able to report any observations. However, the derived stress drops in our data set indicate a break down in earthquake self-similarity. They suggest that within our magnitude range, the increase in magnitude is caused more by increase in slip than by increase in fault dimension.

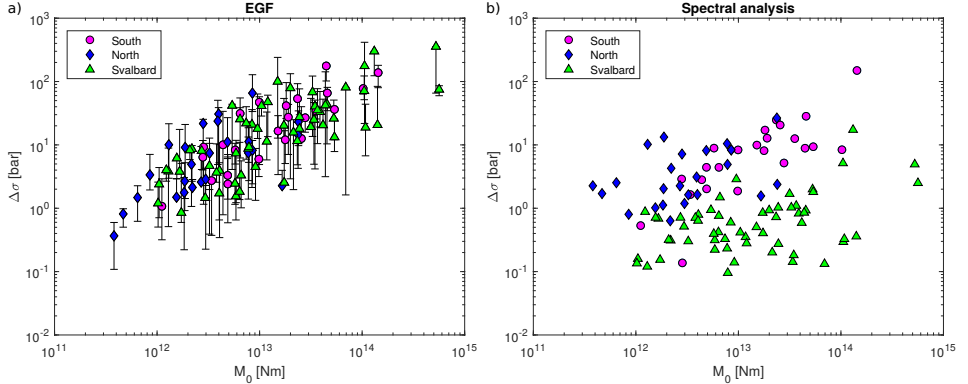


Figure 8: Stress drops obtained for southern Norway (pink dots), northern Norway (blue diamonds) and Svalbard (green triangles) plotted against their seismic moments. Stress drops are derived with the EGF method (a) and with spectral analysis (b). Errorbars in (a) correspond to stress drops with a rise time measurement starting at local minimum and zero amplitude.

For comparison, we obtained stress drops also from spectral analysis (Fig. 8b). These stress drops show no correlation with their corresponding seismic moment and appear to be underestimated for the Svalbard archipelago. Among others, Ide et al. (2003) and Viegas et al. (2010) demonstrated that EGFs remove attenuation effects more efficiently than attenuation correction in spectral analysis. Nevertheless, the standard error of stress drops obtained with the EGF method is estimated to be around 33% and 120% (Abercrombie, 1995; Kaneko & Shearer, 2014). Based on the choice of the starting point of the source time function, we obtain uncertainties in stress drop between 37% and 560%. These uncertainties are derived for individual events. The overall trend of increasing stress drop with increasing seismic moment is statistically robust.

4 Conclusion

This thesis contributes to the knowledge on ambient seismic noise levels, wave propagation and earthquake source parameters in Norway. The main results are:

- High frequency noise varies on a daily basis on average by less than 5 dB. Close to bigger cities the noise increases by up to 15 dB. The variation is relatively low compared to other regions. This is most likely due to the low population density.
- High period noise level variations correlate to weather conditions and to wave heights up to 900 km offshore.
- The theoretical calculated earthquake detection threshold compares well with the smallest observed events and is M_L 1 and 3 in mainland Norway and the Norwegian Sea, respectively.
- Increased ambient seismic noise has a negative influence on the detection threshold, which is demonstrated in the detection threshold map.
- High Lg/Pn amplitude ratios, thus efficient Lg wave propagation, is obtained for mainland Norway.
- The performed tomographic inversion has a resolution limit of 400 km.
- Lg wave attenuation is low onshore and high across the mid-Norwegian Margin.
- Smaller scale variations are observed in the tomographic maps, but they are close to the resolution limit.
- We obtained a large range of stress drop (0.4-355 bar) for Norway, which is comparable with observations in northeastern US.
- The increasing stress drop with increasing seismic moment contradicts earthquake self-similarity in our local magnitude range of 1.3-3.4.

- The stress drops suggest that increase in magnitudes are caused more by increase in slip than by increase in fault dimension.

In conclusion, this thesis contributed to the understanding of the detection limits of the NNSN, wave propagation and the origin of seismic signals. In the future, it is important to continuously evaluate the ambient seismic noise levels as a quality control of the network and the stations. The improved knowledge on Lg wave attenuation and source parameters can be used to derive better seismic hazard maps. The findings and resolution of the Lg wave tomography could be improved in the future with a denser data coverage. This means, in particular, the integration of seismic recordings from other countries. A larger dataset would also strengthen the observations regarding the earthquake source parameters.

5 Publications

Paper 1:

Ambient noise levels and detection threshold in Norway

Andrea Demuth, Lars Ottemöller and Henk Keers

Department of Earth Science,
University of Bergen, Allégaten 41, N-5007 Bergen, Norway

published in Journal of Seismology (2016)

Ambient noise levels and detection threshold in Norway

Andrea Demuth · Lars Ottemöller · Henk Keers

Received: 7 October 2015 / Accepted: 2 March 2016 / Published online: 12 March 2016
© The Author(s) 2016. This article is published with open access at Springerlink.com

Abstract Ambient seismic noise is caused by a number of sources in specific frequency bands. The quantification of ambient noise makes it possible to evaluate station and network performance. We evaluate noise levels in Norway from the 2013 data set of the Norwegian National Seismic Network as well as two temporary deployments. Apart from the station performance, we studied the geographical and temporal variations, and developed a local noise model for Norway. The microseism peaks related to the ocean are significant in Norway. We, therefore, investigated the relationship between oceanic weather conditions and noise levels. We find a correlation of low-frequency noise (0.125–0.25 Hz) with wave heights up to 900 km offshore. High (2–10 Hz) and intermediate (0.5–5 Hz) frequency noise correlates only up to 450 km offshore with wave heights. From a geographic perspective, stations in southern Norway show lower noise levels for low frequencies due to a larger distance to the dominant noise sources in the North Atlantic. Finally, we studied the influence of high-frequency noise levels on earthquake detectability and found that a noise

level increase of 10 dB decreases the detectability by 0.5 magnitude units. This method provides a practical way to consider noise variations in detection maps.

Keywords Seismic ambient noise · Detection threshold · Norway · Seismic network

1 Introduction

Quantification of spatial and temporal variations of seismic noise is important for many aspects of seismology. For example, the ability of a seismic network to detect earthquakes depends on the noise levels at each individual station. Moreover, seismic noise can also be used as signal to evaluate the performance of seismic equipment and vault construction (e.g., de la Torre and Sheehan 2005; Wilson et al. 2002) and it has been used to directly investigate Earth's structure (e.g., Shapiro and Campillo 2004; Sabra et al. 2005). A thorough investigation of seismic noise including quantification of spatial and temporal variations is therefore important.

The most common procedure to compute seismic noise was established by Peterson (1993), who developed a global noise model which is now used as global reference. He defined a new upper (NHNM) and lower (NLNM) noise level boundary in the period range 10^{-1} – 10^5 s. The approach to present seismic noise was extended by McNamara and Buland (2004) who use the whole seismic record, instead of isolating quiet

Electronic supplementary material The online version of this article (doi:10.1007/s10950-016-9566-8) contains supplementary material, which is available to authorized users.

A. Demuth (✉) · L. Ottemöller · H. Keers
Department of Earth Science, University of Bergen,
Allégaten 41, N-5007 Bergen, Norway
e-mail: andrea.demuth@uib.no

periods, and compute probabilities. This makes it possible to present the distribution of noise levels for the entire frequency range over long time periods.

Seismic noise can be caused by human activities, wind, and water waves. Each source generates noise in specific frequency bands. Cultural activity is the main source for increased noise at high frequencies (1–20 Hz), often resulting in strong diurnal variations (e.g., Rastin et al. 2012). Small local earthquakes fall into this frequency band, which means that the cultural noise affects their detectability. Other sources for noise at high frequencies are wind and running water (McNamara and Buland 2004). The seismic noise at intermediate periods of 4–16 s is related to ocean waves (Longuet-Higgins 1950; Hasselmann 1963). In this period range, there are two distinct peaks (McNamara and Buland 2004). The double-frequency peak (periods 4–8 s) is generated by standing gravity waves resulting from superposition of oceanic waves travelling at equal periods in opposite directions. The single-frequency peak (periods 10–16 s) is generated in coastal waters. The vertical pressure variations or *interaction of waves with the shallow sea floor is directly converted into seismic energy* (Hasselmann 1963). While these two peaks are identified on most seismic stations, their amplitudes depend on the distance to the main source area. Pierson and Moskowitz (1964) showed that the peak of the oceanic wave spectrum depends on the maximum wind speed and the length of ocean acted on by the wind. The frequencies of the peaks can be shifted slightly depending on bathymetry and dominant ocean wave period (Marzorati and Bindi 2006).

Various methods exist to quantify earthquake detection thresholds. A common approach is based on the determination of the magnitude of completeness from earthquake catalogues (e.g., Woessner and Wiemer 2005). However, as D'Alessandro et al. (2011a) pointed out, the magnitude of completeness provides no information about spatial distribution of the detection threshold. They therefore propose a more complex evaluation method, SNES, which determines location errors and spatial distribution of earthquake detections. In addition to this, Ringdal (1989) and Kværna and Ringdal (1999) consider the variability of detection thresholds over time. Their continuous threshold monitoring technique provides a way to assess non-detected events, e.g., during the coda of large earthquakes. Schorlemmer and Woessner (2008)

determine a detection probability, based on magnitudes and hypocentres of past earthquakes, whereas Marzorati and Bindi (2006) compare average noise levels with synthetic spectra to derive a spatial variability in the detection threshold.

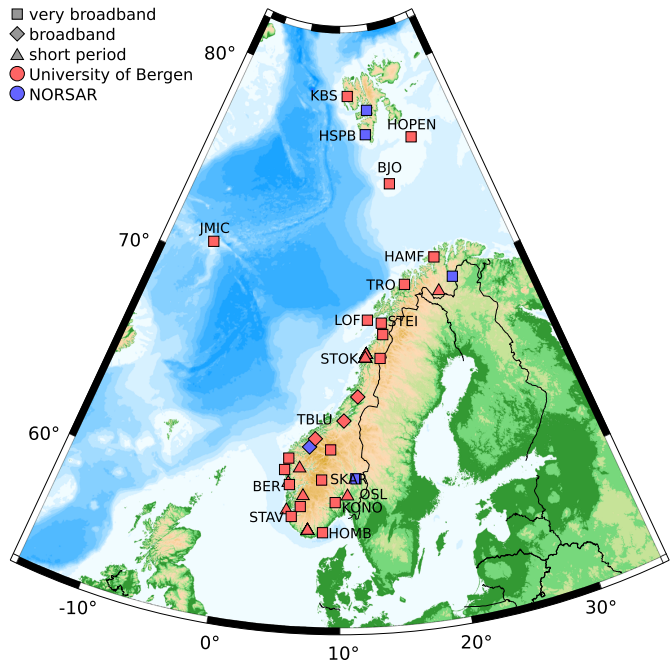
Our main objective in this study is the quantification of ambient seismic noise levels in Norway as well as their temporal and spatial variation. A second objective is to investigate the quantitative relationship between wave height and intermediate period noise levels. Finally, we look at the effect of cultural noise on detection levels using the Norwegian National Seismic Network as an example.

2 Data and noise computation

We evaluate the ambient seismic noise in Norway based on data recorded by the permanent Norwegian National Seismic Network (NNSN) (Fig. 1 and Table 1) as well as two temporary deployments, MAGNUS and NEONOR2. The NNSN consists of 33 stations that are run by the University of Bergen (UoB) and also includes data provided by NORSAR from three seismic arrays and two single seismometer stations. The stations are distributed over mainland Norway, as well as the arctic islands Svalbard, Bear Island, Hopen, and Jan Mayen. All stations are located on bedrock.

The permanent stations are operated by two institutions with different aims, and, therefore the site and vault conditions differ. The majority of the stations operated in Norway were installed in the 1980s and 1990s for use with short period seismometers. The vaults constructed then were shallow, less than 1 m below the surface, but coupled to bedrock. At many of these sites, the short period instruments have been replaced by broadband seismometers, but the vaults remained the same. In 2013, 21 of the seismic stations were equipped with broadband seismometers, mainly Nanometrics Trillium 120 seismometer, and recording was done with Güralp CMG-DM24 digitizers. A deeper vault of about 2 m at station SKAR was built more recently for a broadband sensor. The Svalbard array is equipped with 10-m-deep borehole sensors. The two stations KBS and KONO are part of the Global Seismograph Network (GSN) that have been constructed to produce high-quality data and can thus be used as a reference. KBS on Svalbard has a well

Fig. 1 Map of the Norwegian National Seismic Network. Station codes are only given for stations that are discussed in the text. Very broadband sensors have a natural period of more than 100 s, broadband sensors of 10–60 s, and short period sensors have a natural period of less than 10 s



constructed GSN style vault, while KONO located in southeastern Norway is placed in a tunnel of an abandoned silver mine.

Stations of the MAGNUS and NEONOR2 deployment were placed in existing buildings. During the MAGNUS project, a total of 31 stations recorded in southern Norway for 2 years (2006–2008; Weidle et al. 2010). They used 23 Streckeisen STS2 sensors, 6 Geotech KS2000, and 2 Güralp 40T. The NEONOR2 project deployed a total of 26 stations, 5 Trillium 120, 15 Streckeisen STS2.5, and 6 Güralp 3ESP sensors in northern Norway in 2013. These stations are scheduled to record until April 2016.

When evaluating the noise levels, we have to consider the different installation techniques as, in particular at long periods and for horizontal components, the noise is sensitive to the vault construction (e.g., Vassallo et al. 2012). Shallow vaults, bad insulation, and air circulation also increase long period noise (Díaz et al. 2010; Vassallo et al. 2012; Bormann 2012). Our noise analysis is based on data recorded in 2013. We mainly focus on the NNSN stations, but the analysis of the noise model of Norway includes the temporary networks as well.

We computed noise levels in terms of power spectral density (PSD) with the noise computation implemented in SEISAN (program CONNOI (Ottmøller et al. 2010)), which follows McNamara and Buland (2004). Noise levels are computed for equally spaced log(*f*) values, where interpolation is applied if required. Otherwise, no smoothing across frequencies is applied. We used no overlap for spectrograms and a window length of 15 and 60 min for diurnal and seasonal variations, respectively. Probability density functions (PDFs) are calculated using a 60 min window and 50 % overlap. We calculated the noise levels for all three components. However, for our results, we always use the vertical component.

The PSDs are calculated in decibels with respect to acceleration of $1 \left(\frac{m}{s^2}\right)^2/Hz$ using:

$$P_k = \frac{2\Delta t}{N} |Y_k|^2 \tag{1}$$

The total power P_k is proportional to the square of the amplitude spectra $|Y_k|$. In order to compare the PSD with Peterson (1993), the normalization factor of twice the ratio of the sample interval Δt to the number of samples N is needed. Furthermore, we applied

Table 1 Basic information about the NNSN stations

Station	Latitude [°N]	Longitude [°E]	Location	Vault
AKN	62.18	6.99	Rural, mountain slope	Shallow
ARE0	69.53	25.51	Rural	Deep
ASK	60.47	5.20	Rural	Shallow
BER	60.38	5.33	City	Vault in basement
BJO	74.50	18.99	Arctic island	Shallow
BLS5	59.42	6.45	Rural	Shallow
DOMB	62.07	9.11	Rural	Shallow
FOO	61.59	5.04	Small town	Shallow
HAMF	70.64	23.68	City	Shallow
HOMB	58.27	8.50	City	Shallow
HSPB	77.00	15.53	City	Surface
HOPEN	76.50	25.01	Arctic island	Shallow
HYA	61.16	6.18	Rural	Shallow
JMIC	70.92	-8.73	Arctic island	Deep broadband vault
KBS	78.91	11.91	Arctic island	GSN, deep
KMY	59.20	5.24	Rural	Shallow
KONO	59.64	9.59	Mine tunnel	Very deep
KONS	66.49	13.11	Rural	Shallow
KTK1	69.01	23.23	Rural	Shallow
LOF	68.13	13.54	Rural	Shallow
MOL	62.56	7.54	Rural	Shallow
MOR8	66.28	14.73	Rural	Shallow
NC602	60.74	11.54	Rural	Deep
NSS	64.53	11.96	Rural	Shallow
ODD1	59.91	6.62	Rural	Shallow
OSL	59.93	10.72	City	Vault in basement
SKAR	60.68	8.30	Rural	Deep broadband vault
SNART	58.33	7.20	Rural	Shallow
SPA0	78.18	16.37	Arctic island	Borehole
STAV	58.93	5.70	City	Basement
STEI	67.93	15.24	Rural	Shallow
STOK	66.33	13.01	Rural	Shallow
SUE	61.05	4.76	Rural	Shallow
TBLU	63.41	10.43	City	Basement
TRO	69.63	18.90	City	Museum

a correction factor of ~ 1.143 to account for the used 10 % taper. To analyze the statistical noise variation over a certain time period, we computed PDFs using:

$$P(T_c) = N_{PT_c} / N_{T_c} \quad (2)$$

Here, $P(T_c)$ is the probability for a given center period T_c , N_{PT_c} is the number of spectral estimates that fall

into a 1-dB power bin, and N_{T_c} is the total number of spectral estimates. The mode values of the PDFs were averaged over the frequency ranges 2–10 Hz, 0.5–5 Hz, and 0.125–0.25 Hz. These ranges represent, respectively, the frequencies where the highest signal energy of small local and regional events, teleseismic events, and the double-frequency microseism peak is expected.

3 Temporal noise variation

In this section, we present and evaluate the diurnal and seasonal variations in the seismic noise. Changes in cultural activity are expected to be visible for higher frequencies between day and night. Variations due to seasonal weather changes are expected to be seen at lower frequencies, especially the microseism peaks. All provided times are in UTC and local time. The UTC is in the winter 1 h and in the summer 2 h behind local time.

3.1 Diurnal variations

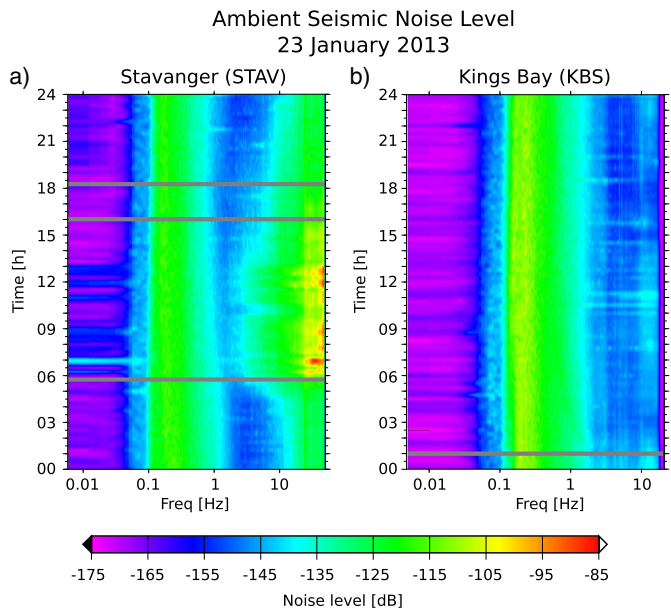
As an example of the difference between a culturally quiet and noisy station, we show in Fig. 2 the 24-h PSD spectrograms of stations KBS and STAV. KBS is installed on the arctic archipelago Svalbard about 1 km from the coast near a small settlement. The station in Stavanger is placed in the basement of a building in an industrial area. Figure 2a shows that the noise levels at STAV for frequencies above 4 Hz increase at 5 a.m. (6 a.m. local time) and decrease again around 4 p.m. (5 p.m. local time), correlating with the daily working hours. KBS (Fig. 2b), on the other hand, shows no obvious variation in this frequency range due to the absence of cultural

activity. Most NNSN stations show a diurnal variation of less than 5 dB (Online Resource 1, Table 1). However, stations located in larger towns, e.g., Stavanger, Trondheim, and Bergen, show variations of up to 15 dB. Furthermore, the daytime cultural noise for these stations is greater during working days than in the weekend.

McNamara and Buland (2004) observed noise variations of 15–20 dB for higher frequencies (1–100 Hz) across the USA. Their lowest diurnal variation was 10 dB. Marzorati and Bindi (2006), who studied noise in northern Italy, observed diurnal variations for frequencies higher than 1 Hz between 10 and 20 dB for different sites. Similar variations were observed by Rastin et al. (2012) for the North Island of New Zealand for a frequency range of 1–10 Hz (diurnal variations: 7–20 dB). Compared to those studies, the NNSN sites in Norway show less diurnal variation. This is partly explained by the sparse population density in Norway compared to the other countries.

The comparison of diurnal variations between January and July (Online Resource 1, Table 1) shows a significantly lower variation in July for the southern sites with a maximum of 8 dB. On the other hand, the northern stations have an increased diurnal variation in July. As an extreme example, Hammerfest has

Fig. 2 Twenty-four-hour PSD spectrogram of the vertical component for **a** STAV and **b** KBS on the 23 January 2013. Time is given in UTC, which is 1 h behind local time



a diurnal noise level variation of 4 dB during January and 10 dB during July. Hence, we observe an increase in the cultural activities in northern Norway only. This is similar to observations by Rastin et al. (2012) in New Zealand for the summer months. Explanations for those observations could be snow coverage and summer holidays in Norway. July is the month of school summer holidays, which reduces regular daily traffic in the southern cities. The snow coverage in northern Norway is a possible reason for noise attenuation during the winter, thus smaller noise levels.

3.2 Seasonal variations

Seasonal variations in noise levels are caused by seasonal changes in the weather (e.g., Stutzmann et al. 2000; Traer et al. 2012) and also depend on the offshore bathymetry (e.g., Longuet-Higgins 1950; Kedar et al. 2008). In order to analyze the seasonal noise variations in Norway, we chose 13 stations, representative for island, coastal, and inland stations (Online Resource 1, Table 2). Figure 3 shows an example of the PSD and the PDF mode values for the summer and winter months for TRO. This station is installed in the basement of a museum in Tromsø.

The most significant noise level variation in the PSD occurs for periods between 1 and 35 s. The noise levels are high in the period October–March (winter) and low in the period April–September (summer). During the summer months, the noise levels stay low, apart from a few individual peaks related to individual storms. The summer and winter modes show that the microseism peaks have different amplitudes and occur at different frequencies, with the peaks shifted by 1–2 s toward shorter periods in the summer. These variations result from rougher weather conditions with longer ocean wave periods during winter (e.g., Bretschneider 1959).

The highest seasonal variation, 7–22 dB, in Norway is observed for low frequencies (0.125–0.25 Hz). This compares to 25 dB reported by Marzorati and Bindi (2006) for a frequency band of 0.1–0.3 Hz in Italy, 15–20 dB ($f \sim 0.125$ Hz) by McNamara and Buland (2004) for the USA, 20 dB ($f \sim 0.111$ Hz) by Díaz et al. (2010) for Iberia and Morocco and 6–10 dB ($f = 0.25$ –1 Hz) by Rastin et al. (2012) for New Zealand.

The noise levels in the winter for the frequency range 0.5–5 Hz are slightly higher (0.24–11.58 dB)

than during the summer (Online Resource 1, Table 2). In the frequency range 2–10 Hz, we observe that half of the analyzed stations have a higher noise level during the summer (0.48–4.88 dB) and the other half during the winter (0.12–19.4 dB). However, the stations with increased noise levels show no geographical pattern. This therefore implies a weather-independent seasonal noise level variation for this frequency range.

4 Weather conditions and ambient seismic noise

In this section, we study the link between ocean waves that result from the weather conditions and the seismic noise levels in northern Norway.

Wind speed (10 m above sea level) and wave height values offshore northern Norway for 2013 were provided by the Norwegian Meteorological Institute. The area covered is [0°–35° E] and [66° N–75° N], with a grid resolution of 10 km and a 3-h time resolution. The wind speed and wave height values are based on the operational model from the European Centre for Medium-Range Weather Forecasts, which is a high resolution numerical weather prediction model (Reistad et al. 2011). The model uses temperature, pressure, wind, specific humidity, and cloud water observations for atmospheric modelling. The ocean wave field is then generated with the wave prediction model coupled to the atmospheric conditions (Reistad et al. 2011).

From these data, we calculated average wind speed and wave height values, as well as local maxima. This was done in 50-km intervals around the corresponding station with a distance increment of 10 km and an azimuth increment of 1°. Given the wave height $w(r, \theta)$, with r distance of the wave to the station and θ the azimuth, we compute the average wave height for each bin using:

$$\bar{w} = \frac{\int_{\theta_1}^{\theta_2} \int_{r_1}^{r_2} w(r, \theta) r dr d\theta}{\int_{\theta_1}^{\theta_2} \int_{r_1}^{r_2} r dr d\theta} \quad (3)$$

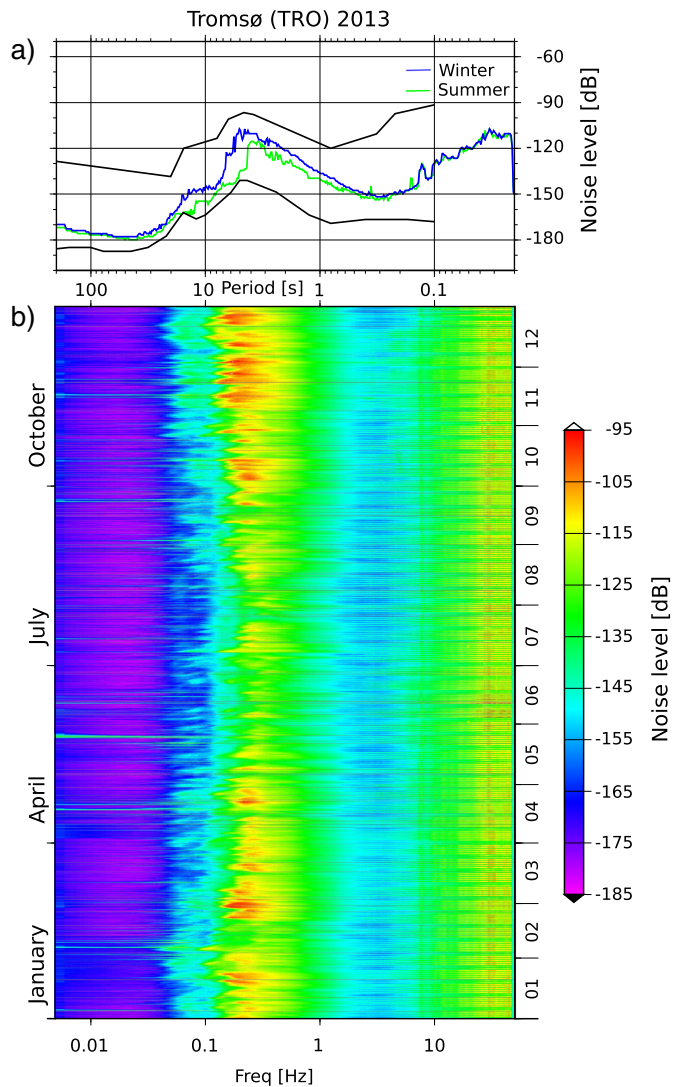
The average wind speed is computed by replacing wave height by wind speed in Eq. 3. Figure 4 shows the wave height and wind speed maps for northern

Norway on March 16th 2013 at 9 a.m. This figure also shows the 24-hour PSD spectrogram at station TRO on that day. A low-pressure weather system was moving toward the coast of Norway (at 9 a.m. centered at $\sim 74^\circ$ N and $\sim 15^\circ$ E). The spectrogram shows that the noise level around the double-frequency peak at about 4–7 s (0.143–0.25 Hz) increases very clearly from -115 dB at 9 a.m. to -100 dB at midnight.

Ardhuin et al. (2012) suggest that noise at a single station can be related to an area averaged wave

height. We investigate this by comparing average wind speeds and average wave heights at various distance ranges with the noise levels in our three frequency bands. Figure 5a, b show this comparison for average wave heights between 250 and 300 km away from the station and average wind speeds of 50–100 km distance over 10 days for the stations LOF and HAMF. We chose large offshore distances with a high correlation coefficient between noise and weather conditions. Both stations reveal a strong correlation of

Fig. 3 **a** PDF mode values for winter and summer 2013. The *solid black lines* show the NHNM and NLNM of Peterson (1993), respectively. **b** PSD spectrogram of 2013. Both plots were calculated for the vertical component of station TRO



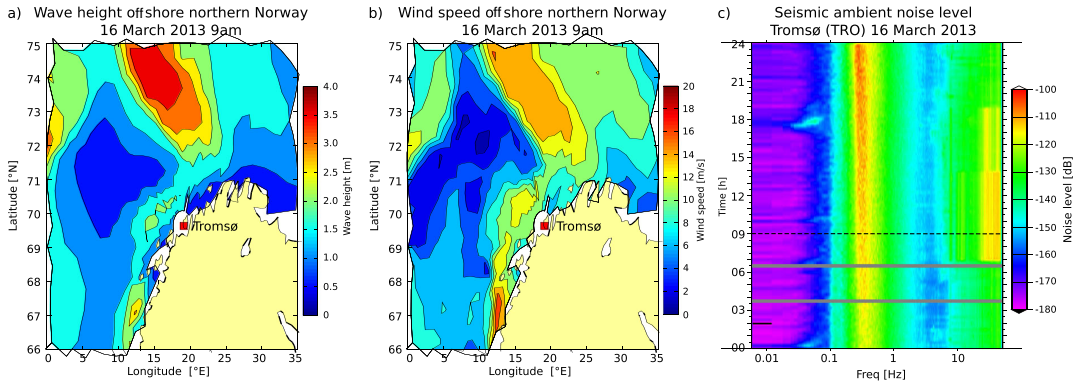


Fig. 4 Modeled **a** wave height and **b** wind speed offshore northern Norway on March 16th 2013 at 9 a.m. Both wave height and wind speed scale are given on the y-axis to the right,

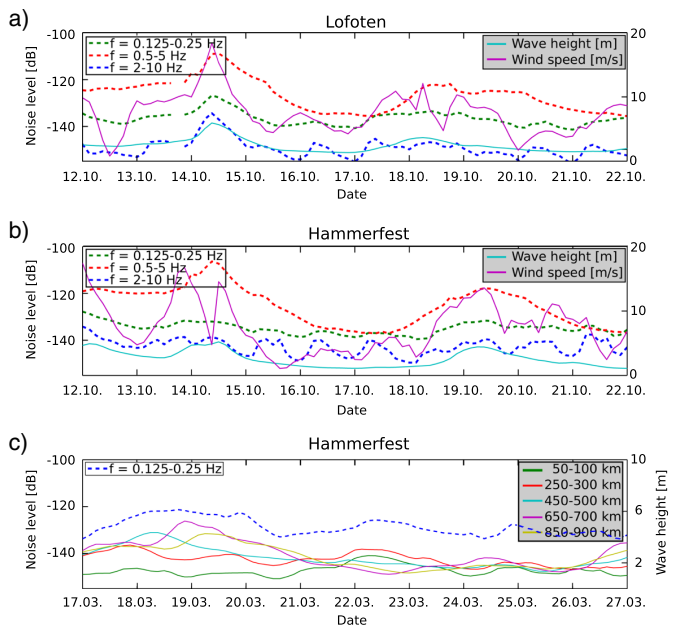
where the units are m and m/s, respectively. **c** Twenty-four-hour PSD spectrogram of Tromsø vertical component for March 16th 2013

$r_{LOF} = 0.84$ and $r_{HAMF} = 0.79$ (Online Resource 1, Table 3) between wave heights and noise levels in the low-frequency band (0.125–0.25 Hz). We also find that the peak in time for higher frequencies correlates with the wave height peak.

Resource 1, Table 3) with the noise at high frequencies (2–10 Hz). An additional reason for the strong correlation at LOF could be its position on a peninsula. The effect of wind on the higher frequency noise depends both on the conditions around the site and the burial depth of the seismometer (e.g., Carter et al. 1991; Bormann 2012). This correlation is for example not clearly observed for station HAMF (Online Resource

For station LOF, which has a shallow vault with a depth of less than 1 m, the wind speed shows an expected high correlation of $r = 0.62$ (Online

Fig. 5 Relationship of seismic ambient noise levels of the vertical component and average wave heights at defined distances for **a** Lofoten and **b** Hammerfest in October. Wave heights are averaged over the distance of 250–300 km away from the corresponding station. Wind speeds are averaged over a distance of 50–100 km. **c** Seismic ambient noise levels of frequencies 0.125–0.25 Hz compared to average wave heights at various distance ranges in March



1, Table 3). Other stations near the coast show a similar relationship between average wind speeds and noise levels for frequencies 0.5–5 and 2–10 Hz. Seismic noise due to wind attenuates quickly and thus is predominantly generated near the seismic station. Carter et al. (1991) showed high-frequency noise as function of depth and found that prevalent wind generated noise at the surface. Subsurface stations recorded no noise for frequencies above 3 Hz. However, seismic noise generated in the ocean over large areas results from a combination of weather conditions (e.g., Bormann 2012).

We are also interested in evaluating the distance to the station for which wave height data have an effect on the seismic noise levels, thus can be used as a proxy. Figure 5c presents the low-frequency noise levels together with the wave heights for various distance ranges. Using data in the period March 17th–27th 2013 reveals that the link between wave height and noise is strongest when considering near-coastal wave heights. However, wave heights up to 900 km offshore can be used as a proxy to estimate noise levels closer to the coast (see Online Resource 1, Table 4). Since wave height levels at various distances are not independent from each other, as seen in Fig. 5c,

evaluation of the correlation allows no general conclusion that wave heights at larger distances influence the observed noise levels. Nevertheless, our average wave height values at 850–900 km offshore have a correlation coefficient of 0.73 (Online Resource 1, Table 4) with noise levels for low frequencies in the year 2013. Thus, our observations agree with Arduin et al. (2011), who proposed that reflections within 1000 km offshore increase the seismic noise level for the double-frequency peak.

While the link between the microseism peaks and ocean wave heights is well established (e.g., Bromirski et al. 2005; Arduin et al. 2012), we also tested the link in our intermediate frequency band. Figure 6 shows the noise levels at frequencies 0.5–5 Hz against the average wave heights for various distances from the station HAMF and LOF together with the corresponding correlation coefficients. For distances up to 600 km offshore, we observe a strong correlation ($r > 0.7$) between increasing wave heights and increasing noise levels. With increasing distance, the correlation becomes more scattered. We also see a correlation for higher frequencies (2–10 Hz), which may be due to increased wind speeds that correlate with wave heights.

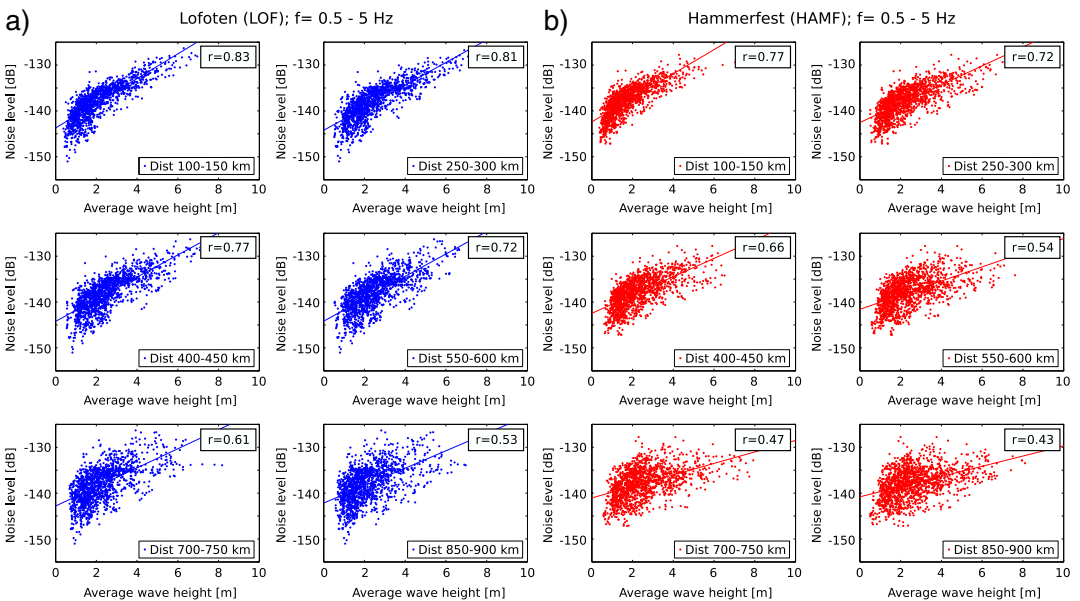


Fig. 6 Relationship of seismic ambient noise levels of the vertical component and average wave heights for six distance ranges for **a** Lofoten and **b** Hammerfest. Correlation coefficients are shown in the upper right insets

Instead of using wave heights averaged over a distance interval to estimate the change in noise levels, it would also be possible to use the maximum wave height within a distance range. To test which of the two is a better proxy, we made a comparison in Fig. 7. The dependency of noise levels on the local maximum wave height is slightly higher (see Fig. 7 for correlation coefficients). As the maximum is slightly easier to estimate, the local wave height maximum is a good approximation for the noise level wave height relation, even though the noise is expected to be generated over a larger area, as suggested by Ardhuin et al. (2012), for regions such as north-western Europe.

5 Noise model for Norway

Another factor of importance in this study is the geographic noise variation. For frequencies around the microseism peaks, this can be related to differences in the natural ambient noise. At frequencies lower than the single frequency peak, the individual station noise mostly represents the seismic station setup (Bormann 2012). For the higher frequencies, the noise largely

reflects the proximity to cultural activity. To evaluate the performance of a seismic station and to identify needs for improvement, it is crucial to develop a local noise model.

In order to assess the geographic noise distribution, the average mode values of the individual stations are shown in Fig. 8. This was done for all three of our chosen frequency ranges for day and night time in January and July. Additionally, we included mode values of temporary stations from the MAGNUS project (July 2007; January 2008) and the NEONOR2 project (January 2014). The temporary stations generally show higher noise levels than the nearby permanent station. This was expected, largely due to the fact that the temporary stations are installed inside buildings. The comparison of day versus night and January versus July (Fig. 8) reflects our above-mentioned observations. We have higher noise levels in the frequency range 2–10 Hz during the day for city stations and higher noise levels in the frequency range of 0.125–0.25 Hz in January.

Figure 8c suggests that stations in southern Norway have slightly lower noise levels than the northern stations for the frequency band 0.125–0.25 Hz. This

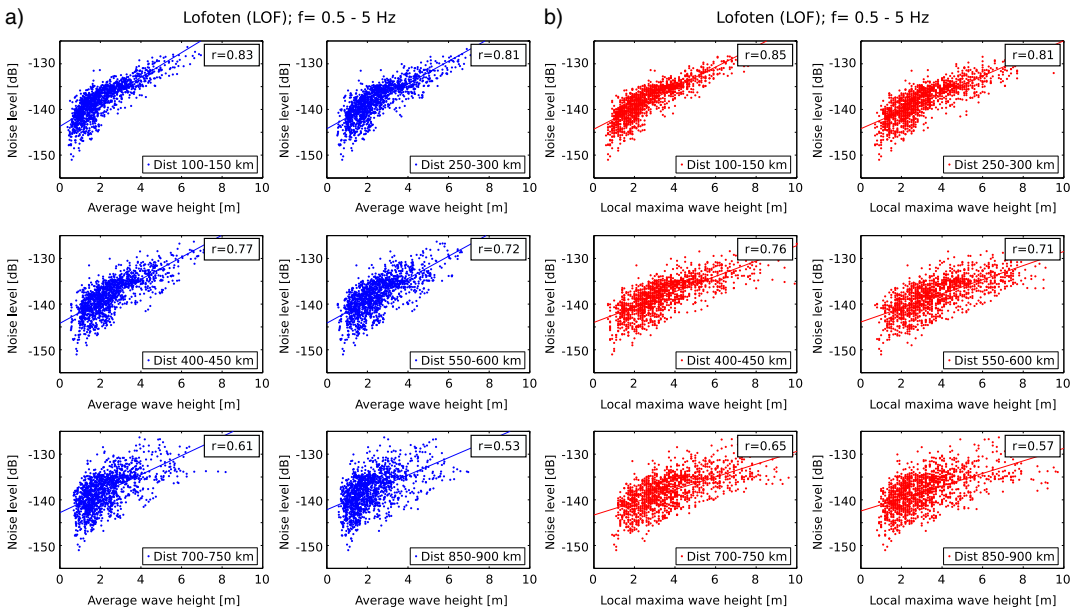


Fig. 7 Relationship of seismic ambient noise levels of the vertical component and wave heights for six distance ranges for Lofoten. **a** Noise levels versus average wave heights. **b**

Noise levels versus local maxima wave heights. Correlation coefficients are shown in the upper right insets

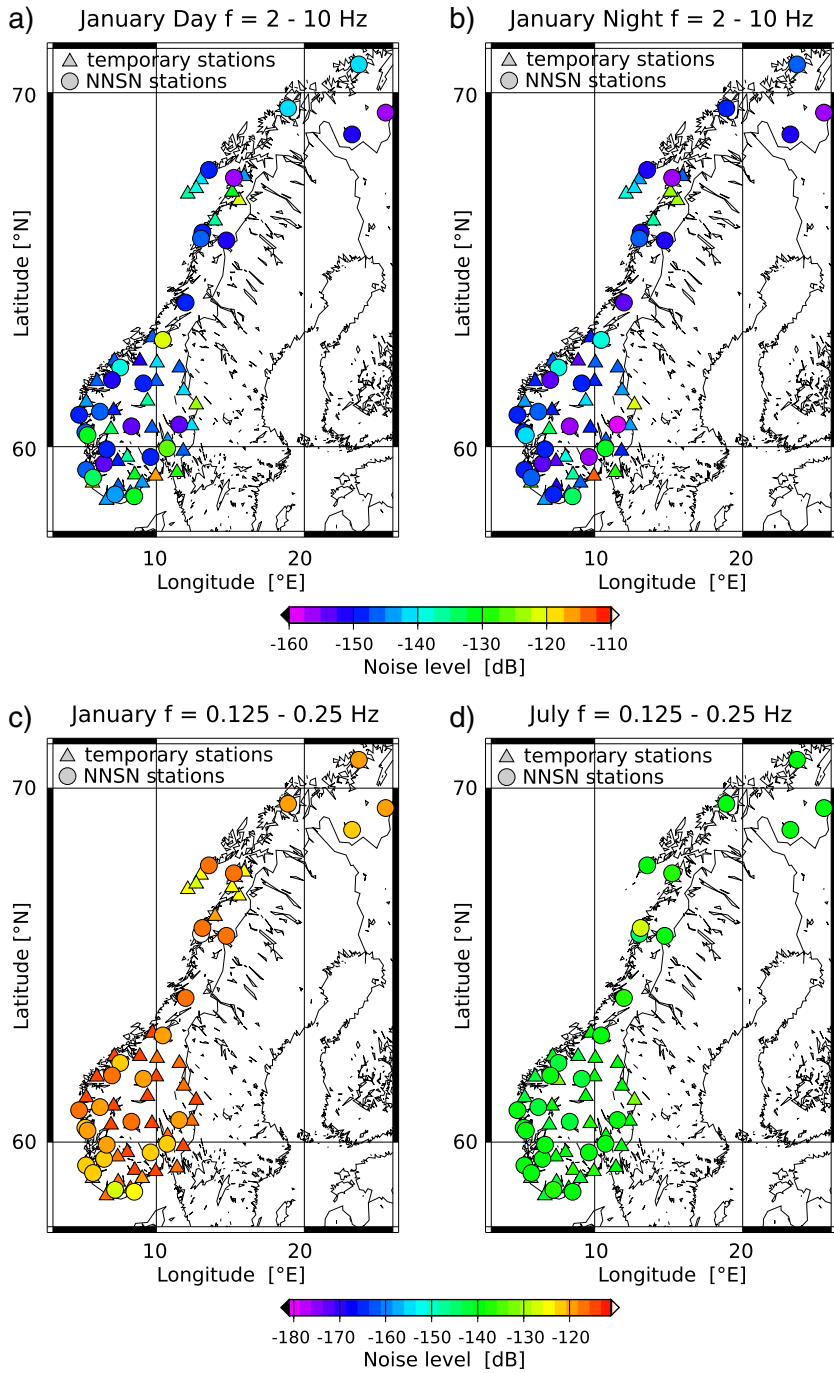


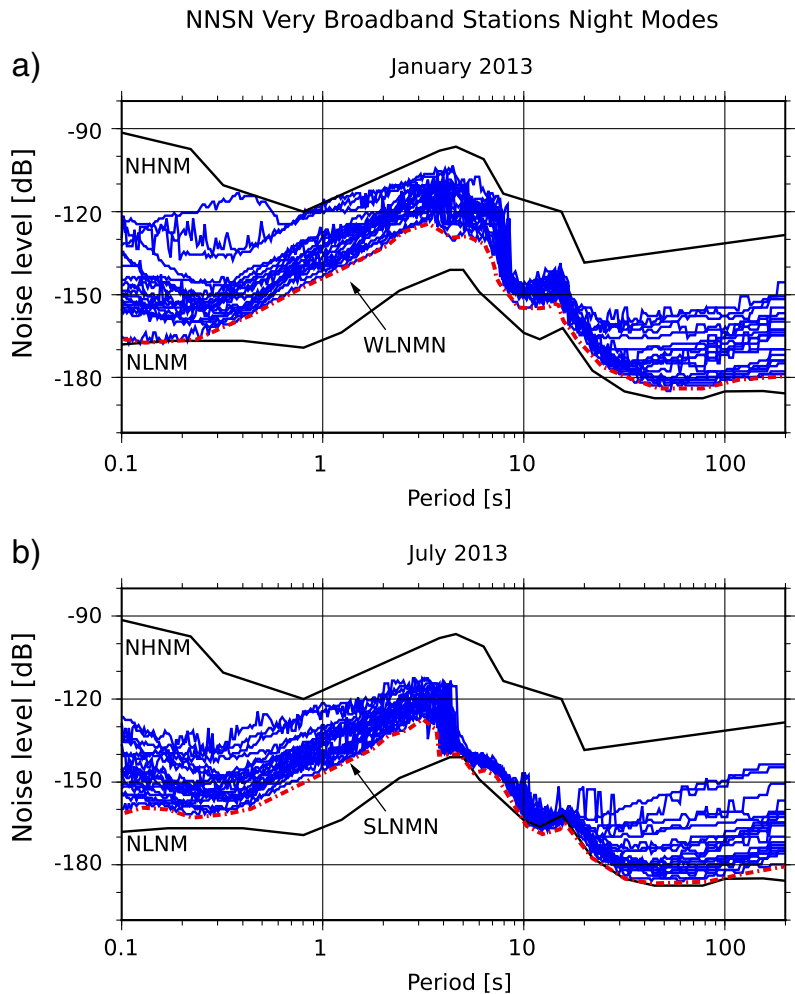
Fig. 8 Geographic noise distribution of the vertical component in Norway. Comparison of **a** day and **b** night in January 2013 for frequencies 2–10 Hz. Noise level variations between **c** January and **d** July are shown for frequencies 0.125–0.25 Hz

can be explained by the larger distance to the dominant noise source regions in the northern Atlantic. The noise levels hardly vary between stations in July for this frequency range (Fig. 8d). We could have expected to find that stations near the coast have higher microseism peak amplitudes, but that difference is not significant. Overall, the noise level variation in Norway shows no clear geographic pattern. This may be the result of low attenuation and an indication that the geology has no significant effect on the regional noise pattern.

The best case scenario of the network performance is given by the low noise summer and winter models for Norway (SLNMN, WLNMN; Fig. 9). They are constructed from the minimum mode values of most very broadband stations. Two stations of the network had to be omitted due to technical problems in the analyzed time period.

The shape of both curves are in good agreement with each other as well as with the Peterson (1993) model for periods shorter than 1 s and longer than 20 s. We observe a shift of the single- and double-

Fig. 9 Low noise model for Norway (LNMN) constructed from the minimum mode values of the vertical component from most very broadband stations of the NNSN. The red line marks the lowest noise levels in Norway for night time (6 p.m.–6 a.m.) in **a** January 2013 and **b** July 2013



frequency peak toward longer periods in January as explained in the discussion of Fig. 3. An increased scattering between stations and higher noise levels for periods between 1 and 20 s is observed in January. This period band includes the microseism peaks. As discussed in the weather section, weather conditions are rougher during the winter months. This causes higher scattering in the observation. The local maxima around 6 s are significantly lower in July.

Various studies observe a splitting in the double-frequency peak (e.g., Stephen et al. 2003; Bromirski et al. 2005; Kuper and Burlacu 2015). Bromirski et al. (2005) distinguish between short (2–5 s) and long (5–11 s) double-frequency peaks. They assume a nearby local storm source for the short period peak and larger storms in the open ocean as sources for the longer period peak. If the same applies to Norway, the noise levels in Norway caused by local storms are more stable than the ones triggered by distant storms.

Noise levels at longer periods are partly related to the vault construction and seismometer self-noise (McNamara and Buland 2004). We find that the best constructed stations in Norway (KONO, KBS, SKAR) perform well for all their components, but for shallow vaults, the range of observations is quite large. The highest noise levels at long periods are observed for HOMB, HOPEN, and STAV. This is not surprising, since the vault and site conditions for these stations are not favorable.

To quantify the noise level variation between stations, we calculated the average mode of all mainland and island stations, respectively, and subtracted the individual mode values (Online Resource 1, Tables 5 & 6). This was done for the three frequency ranges. The highest variation of 26 dB between mainland stations is observed in January for the frequency range 2–10 Hz between OSL and STEI. STEI has a 10-dB lower noise level for those frequencies than the average. We observed a noise level variation of approximately 16 dB between the quietest and noisiest mainland station for the frequency range 0.5–5 Hz and 9 dB for frequencies 0.125–0.25 Hz. In July, we observed similar variations of 15 dB and 24 dB for the frequency ranges 0.5–5 Hz and 2–10 Hz. The noise level variation for the frequency range 0.125–0.25 Hz is 8 dB higher in July (17 dB) than in January.

The variance of noise levels between island and mainland stations is stable in January and July for all frequency ranges. The average noise value of island

stations in the frequency range 0.125–0.25 Hz is the same as for mainland stations. For the other two frequency ranges, we observe 6–8 dB higher average noise levels at the island stations. The highest noise level variation of 38 dB between stations is observed for the frequency range 2–10 Hz. The overall noisiest stations are JMIC and HOPEN, whereas SPA0 is the quietest station. Higher noise levels, as observed for OSL and JMIC, make earthquake analysis (teleaseismic, local, and regional) more difficult. Lower noise levels, as, e.g., recorded by STEI and SPA0, contribute to the detectability of smaller earthquakes.

6 Effect of noise on detection threshold

So far, we focused on the characterization of ambient noise and the evaluation of seismic station performance. In this final section, we discuss the effect of noise on seismic observations.

It is quite obvious that the detection of earthquakes and the observation of seismic phases depend on the noise levels at a station. In principle, one also expects to find larger travel time residuals for seismic phases observed on noisier stations. This could not be confirmed from the NNSN earthquake catalogue. A possible reason for this is the practice of only reading phases when the signal to noise ratio is high enough. Also, the increase in arrival time error due to noise is likely to be smaller than the error caused by the velocity model that was used.

A second important observable is the detection level. The detection levels for Norway were calculated based on the requirement to have four detecting stations. In this case, the detection level is given by the magnitude that can be seen by the most distant of the four stations. The magnitude–distance relationship derived from the NNSN earthquake catalogue of the past 25 years is:

$$M_L(d) = 0.5 + 0.004d. \quad (4)$$

In other words, at distance d (in km), a magnitude M_L can be detected. We computed a threshold map for Norway (Fig. 10b) by simply computing the minimum expected magnitude at the fourth nearest station for each grid point using Eq. 4. For this, we included stations from other networks, where we have data access.

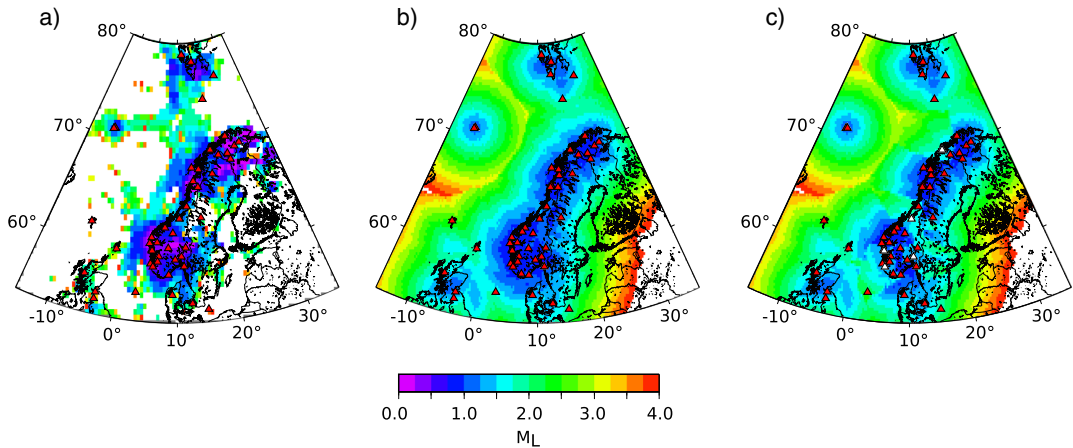


Fig. 10 **a** Smallest local magnitude observed by the NNSN. **b** Synthetically calculated detection threshold for Norway. **c** Implementing day noise levels in the synthetic detection threshold of the vertical component for stations marked in *white*

Our detection levels are defined by the network geometry and the expected detection level is based on the earthquake catalogue. This is similar to Schorlemmer and Woessner (2008), who derived detection thresholds for southern California based on station locations and event magnitudes. They calculated the detection probability of an event at a certain station and used this to derive a threshold map. A more complex approach to assess the detectability of earthquakes by seismic networks was published by D’Alessandro et al. (2011a). They focused on the spatial detectability of a given magnitude and considered the spatial noise level variations, the velocity model used and the accuracy of the earthquake detection in time and space. We argue that our simple approach gives a first order estimate of detection levels and allows for easy incorporation of noise level variation between stations. Our computed detection thresholds (Fig. 10b) compare well to the smallest local magnitudes observed (Fig. 10a).

The synthetic map reveals a local magnitude detection threshold for mainland Norway of $M_L = 1$, whereas the detection threshold in the Norwegian Sea is as high as magnitude 3. In other places, work based on the methodology by D’Alessandro et al. (2011a) found a threshold magnitude of mainly 2–2.5 for mainland Italy (D’Alessandro et al. 2011a), 1.8 for Greece (D’Alessandro et al. 2011b), and 1.4 for Alaska (D’Alessandro and Ruppert 2012). The coastal areas in Italy and Greece have detection thresholds of

a magnitude around 2.5. While this gives an indication that our numbers are comparable to other networks, network geometry, station performance, and seismic attenuation can result in significant differences.

The noise level variations determined in the previous sections are used to calculate variabilities in earthquake detection.

$$\Delta M_L = \log|a_1(t_i)/a_2| \quad (5)$$

For this purpose, we calculated the ratio of the average peak amplitude of a seismogram (a_2) and the peak amplitude (a_1) at a specific time t_i . Equation 5 provides us with variations in magnitude detectability. The peak amplitudes a_1 and a_2 in Eq. 5 are derived from the power spectral values (P) over a frequency range $|f_S, f_E|$ using:

$$a = 1.25\sqrt{P(f_E - f_S)} \quad (6)$$

Havskov and Alguacil (2004) and Peterson (1993). Therefore, we have a relation between the variation in local magnitude detectability and noise levels. For an increase in noise levels of 10 dB, the detectability of earthquakes decreases by a local magnitude of 0.5.

The above presented variations in noise levels this relation provide us with the following observations:

- Detection level of local and regional earthquakes in bigger cities during the day increases by up to 0.75 units of local magnitude

- Seasonal noise variation changes the detectability of teleseismic events by 0.25 units of magnitude
- Detectability of regional and local events of individual stations can vary by two units of magnitude
- Detectability of teleseismic events can vary up to 1.5 units of magnitude (e.g., an increase in the average wave height level of 4 m at a distance of 100–150 km decreases the detectability of teleseismic events at HAMF by approximately 0.5 orders of magnitude Fig. 6)

The translation of difference in noise into magnitude provides a simple way to consider noise variation in detection maps. The impact of increased noise levels on the detection threshold of Norway is shown in Fig. 10c. In that figure, we increased the detection threshold of stations with the highest day and night noise level variation (OSL, STAV, BER, TBLU, TRO) by 0.5 units of magnitude. The increase of detectability influences especially the detection threshold in the offshore areas. The higher threshold in the offshore areas caused by the higher noise levels around STAV and TBLU is reflected in the observed earthquake catalogue (Fig. 10a).

7 Conclusion

We have computed the ambient seismic noise levels for Norway to investigate temporal and spatial noise variation, and to develop a local noise model. The daily noise level variations correlate with cultural activity mostly in the bigger cities. The differences in cultural seismic noise between stations were considered in the computation of detection maps, confirming that high noise levels have a significant negative effect on earthquake detection. Comparison with the smallest observed magnitudes from the earthquake catalogue shows that a fairly simple approach provides useful results that can be used to plan modifications to a seismic network. We evaluate the strong correlation between seismic noise and weather conditions for Norway. We showed in particular that local wave height maxima are a good approximation for the noise level wave height relation and that wave height variations closer to the stations have a stronger influence on the noise level. We quantified the relation between wave height and noise levels at frequencies around the double-frequency peak. No clear geographical pattern

of noise level variation could be found for Norway, indicating that the ocean-generated noise propagates quite efficiently in this area. Using the mode noise levels of most very broadband stations in Norway, we constructed a low-noise model for January and July 2013. The comparison of noise levels between stations allowed us a performance evaluation of the network. Thus, monitoring of seismic noise over time provides an excellent quality control measurement.

Acknowledgments We thank the anonymous reviewers for their constructive comments, which improved the revised manuscript. We thank Magnar Reistad for providing us with weather data from the Norwegian Meteorological Institute. This work was carried out under the NNSN project that is financially supported by the Norwegian Oil and Gas Association.

Open Access This article is distributed under the terms of the Creative Commons Attribution 4.0 International License (<http://creativecommons.org/licenses/by/4.0/>), which permits unrestricted use, distribution, and reproduction in any medium, provided you give appropriate credit to the original author(s) and the source, provide a link to the Creative Commons license, and indicate if changes were made.

References

- Ardhuin F, Stutzmann E, Schimmel M, Mangeney A (2011) Ocean wave sources of seismic noise. *J Geophys Res* 116:C09,004. doi:10.1029/2011JC006952
- Ardhuin F, Balanche A, Stutzmann E, Obrebski M (2012) From seismic noise to ocean wave parameters: General methods and validation. *J Geophys Res* 117:C05,002. doi:10.1029/2011JC007449
- Bormann P (2012) New manual of seismological observatory practice. IASPEI, doi:10.2312/GFZ.NMSOP-2
- Bretschneider C (1959) Wave variability and wave spectra for wind-generated gravity waves. Tech. Memo 118. Beach Erosion Board, Washington D.C
- Bromirski P, Duennebiefer F, Stephen R (2005) Mid-ocean microseisms. *Geochem Geophys Geosyst* 6:Q04,009. doi:10.1029/2004GC000768
- Carter J, Barstow N, Pomeroy P, Chael E, Leahy P (1991) High-frequency seismic noise as a function of depth. *Bull Seismol Soc Am* 4:1101–1114
- D’Alessandro A, Ruppert N (2012) Evaluation of location performance and magnitude of completeness of the Alaska Regional Seismic Network by the SNES method. *Bull Seismol Soc Am* 102(5):2098–2115. doi:10.1785/0120110199
- D’Alessandro A, Luzio D, D’Anna G, Mangano G (2011a) Seismic network evaluation through simulation: an application to the Italian National Seismic Network. *Bull Seismol Soc Am* 101(3):1213–1232. doi:10.1785/0120100066
- D’Alessandro A, Papanastassiou D, Baskoutas I (2011b) Hellenic unified seismological network: an evaluation of

- its performance through SNES method. *Geophys J Int* 185:1417–1430. doi:[10.1111/j.1365-246X.2011.05018.x](https://doi.org/10.1111/j.1365-246X.2011.05018.x)
- Díaz J, Villaseñor A, Morales J, Pazos A, Córdoba D, Pulgar J, García-Lobón J, Harnafi M, Carbonell R, Gallart J, Group TSW (2010) Background Noise Characteristics at the Iber-Array Broadband Seismic Network. *Bull Seismol Soc Am* 100:618–628
- De la Torre TL, Sheehan AF (2005) Broadband seismic noise analysis of the Himalayan Nepal Tibet seismic experiment. *Bull Seismol Soc Am* 95(3):1202–120. doi:[10.1785/0120040098](https://doi.org/10.1785/0120040098)
- Hasselmann K (1963) A statistical analysis of the generation of microseisms. *Rev Geophys* 1:177–209
- Havskov J, Alguacil G (2004) Instrumentation in Earthquake Seismology. Springer
- Kedar S, Longuet-Higgins M, Webb F, Graham N, Clayton R, Jones C (2008) The origin of deep ocean microseisms in the North Atlantic Ocean. *Proc R Soc A* 464:777–793. doi:[10.1098/rspa.2007.0277](https://doi.org/10.1098/rspa.2007.0277)
- Kuper K, Burlacu R (2015) The fine structure of double-frequency microseisms recorded by seismometers in North America. *J Geophys Res Solid Earth* 120(3):1677–1691. doi:[10.1002/2014JB011820](https://doi.org/10.1002/2014JB011820)
- Kværna T, Ringdal F (1999) Seismic threshold monitoring for continuous assessment of global detection capability. *Bull Seismol Soc Am* 89(4):946–959
- Longuet-Higgins M (1950) A theory of the origin of microseisms. *Phil Trans R Soc* 243:1–35
- Marzotari S, Bindi D (2006) Ambient noise levels in north central Italy. *Geochem Geophys Geosyst* 7:Q09,010. doi:[10.1029/2006GC001256](https://doi.org/10.1029/2006GC001256)
- McNamara D, Buland R (2004) Ambient noise level in the continental United States. *Bull Seismol Soc Am* 94:1517–1527
- Ottmøller L, Voss p, Havskov J (2010) Seisan earthquake analysis software
- Peterson J (1993) Observation and modeling of seismic background noise. *US Geol Surv Tech Rept* 93-322:1–95
- Pierson W, Moskowitz L (1964) A proposed spectral form for fully developed wind seas based on the similarity theory of S.A Kitaigorodskii. *J Geophys Res* 69(24):5181–5190
- Rastin S, Unsworth C, Gledhill K, McNamara D (2012) A detailed noise characterization and sensor evaluation of the north island of New Zealand using the PQLX data quality control system. *Bull Seismol Soc Am* 102:98–113
- Reistad M, Breivik Ø, Haakenstad H, Aarnes O (2011) A high-resolution hindcast of wind and waves for the North Sea, the Norwegian Sea, and the Barents Sea. *J Geophys Res* 116:C05,019. doi:[10.1029/2010JC006402](https://doi.org/10.1029/2010JC006402)
- Ringdal F (1989) Multi-channel processing approach to real time network detection, phase association, and threshold monitoring. *Bull Seismol Soc Am* 79(6):1927–1940
- Sabra K, Gerstoft P, Roux P, Kuperman W (2005) Surface wave tomography from microseism in Southern California. *Geophys Res Lett* 32(14):L14,311. doi:[10.1029/2005GL023155](https://doi.org/10.1029/2005GL023155)
- Schorlemmer D, Woessner J (2008) Probability of detecting an earthquake. *Bull Seismol Soc Am* 98:2103–2117
- Shapiro N, Campillo M (2004) Emergence of broadband Rayleigh waves from correlations of the ambient seismic noise. *Geophys Res Lett* 31(7):L07,614. doi:[10.1029/2004GL019491](https://doi.org/10.1029/2004GL019491)
- Stephen R, Spiess F, Collins J, Hildebrand J, Orcutt J, Peal K, Vernon F, Wooding F (2003) Ocean seismic network pilot experiment. *Geochem Geophys Geosyst* 4(10). doi:[10.1029/2002GC000485](https://doi.org/10.1029/2002GC000485)
- Stutzmann E, Roult G, Astiz L (2000) GEOSCOPE Station noise levels. *Bull Seismol Soc Am* 90(3):690–701. doi:[10.1785/0119990025](https://doi.org/10.1785/0119990025)
- Traer J, Gerstoft P, Bromirski P, Shearer P (2012) Microseisms and hum from ocean surface gravity waves. *J Geophys Res* 117(B11307). doi:[10.1029/2012JB009550](https://doi.org/10.1029/2012JB009550)
- Vassallo M, Festa G, Bobbio A (2012) Seismic ambient noise analysis in southern Italy. *Bull Seismol Soc Am* 102(2):574–586. doi:[10.1785/0120110018](https://doi.org/10.1785/0120110018)
- Weidle C, Maupin V, Ritter J, Kværna T, Schweizer J, Balling N, Thybo H, Faleide J, Wenzel F (2010) MAGNUS—a seismological broadband experiment to resolve crustal and upper mantle structure beneath the southern Scandes mountains in Norway. *Seismol Res Lett* 81(1):76–84. doi:[10.1785/gssrl.81.1.76](https://doi.org/10.1785/gssrl.81.1.76)
- Wilson D, Leon J, Aster R, Ni J, Schlue J, Grand S, Semken S, Baldrige S, Gao W (2002) Broadband seismic background noise at temporary seismic stations observed on a regional scale in the southwestern United States. *Bull Seismol Soc Am* 92(8):3335–3342. doi:[10.1785/0120010234](https://doi.org/10.1785/0120010234)
- Woessner J, Wiemer S (2005) Assessing the quality of earthquake catalogues: estimating the magnitude of completeness and its uncertainty. *Bull Seismol Soc Am* 95(2):684–698. doi:[10.1785/0120040007](https://doi.org/10.1785/0120040007)

Electronic supplementary material 1 - Tables**Ambient noise levels and detection threshold in Norway**

by Andrea Demuth, Lars Ottemöller, Henk Keers

Corresponding author: A. Demuth,
 Department of Earth Science, University of Bergen, Allégaten 41, N-5007 Bergen,
 Norway; Tel.: +47-55583661, E-mail: Andrea.Demuth@uib.no

Table 1 Diurnal noise level variation of the vertical component of mainland stations for given time and frequency ranges ($f_1=0.125-0.25$ Hz; $f_2=0.5-5$ Hz; $f_3=2-10$ Hz). The numbers are given in dB. Day time is considered to be between 6 am and 6 pm.

Station	January			July		
	f_1	f_2	f_3	f_1	f_2	f_3
AKN	0.54	1.04	2.62	0.12	0.82	1.78
ARE0	0.92	0.20	0.20	0.54	0.00	0.86
ASK	0.40	1.50	3.42	0.14	1.50	1.40
BER	0.22	3.96	9.24	0.60	3.22	7.36
BLS5	0.68	0.34	1.06	0.38	0.88	2.00
DOMB	0.48	0.44	1.24	1.24	1.18	3.12
HAMF	0.06	0.36	4.48	0.34	3.10	10.36
HOMB	0.26	0.18	0.08	0.18	0.38	0.56
HYA	0.26	0.80	1.62	0.38	1.70	1.16
KMY	0.14	1.40	2.70	0.56	0.08	0.64
KONO	0.54	2.34	6.70	0.76	2.68	5.76
KONS	0.12	0.46	0.70	0.66	2.84	1.42
KTK1	1.20	0.46	0.26	1.78	0.62	0.98
LOF	1.44	0.10	2.34	2.20	3.08	4.48
MOL	0.30	0.00	0.00	0.36	0.38	0.02
MOR8	0.14	0.44	1.12	2.14	1.58	2.18
NC602	0.32	1.46	4.58	0.18	2.28	4.84
NSS	0.36	2.22	4.54	1.46	3.04	4.52
ODD1	0.50	0.02	0.30	1.22	0.22	0.80
OSL	0.02	4.54	6.56	1.62	5.52	7.64
SKAR				0.10	1.26	3.58
SNART	0.86	0.78	1.90	0.08	1.16	1.78
STAV	0.62	6.92	14.50	1.06	2.44	7.10
STEI	0.94	0.24	0.98	1.06	2.00	2.18
SUE	0.10	0.04	0.22	1.02	0.98	1.62
TBLU	0.14	6.24	13.22	0.22	5.16	8.32
TRO	0.56	2.96	7.04	0.12	3.58	10.20

Table 2 Seasonal noise level variation 2013 of the vertical component for given frequency ranges ($f_1=0.125-0.25$ Hz; $f_2=0.5-5$ Hz; $f_3=2-10$ Hz). The numbers represent the average noise level of the whole year minus the noise level of the summer months April till September in dB.

Station	f_1	f_2	f_3
BJO	15.54	4.32	7.36
DOMB	17.52	0.46	4.02
HAMF	17.08	2.90	0.48
HOMB	6.88	1.16	0.12
HSPB	10.70	1.68	1.48
JMIC	19.60	3.28	6.80
KBS	14.22	0.88	1.76
KONO	17.44	0.90	2.74
LOF	17.10	3.32	1.66
MOR8	15.44	1.92	1.02
NSS	14.78	0.24	4.88
SKAR	18.12	2.38	1.26
SUE	21.72	11.58	19.40
TRO	18.34	3.48	0.44

Table 3 Correlation coefficient between the noise levels for given frequency ranges ($f_1=0.125-0.25$ Hz; $f_2=0.5-5$ Hz; $f_3=2-10$ Hz) and wind speed and wave height values at station LOF and HAMF for the year 2013.

	f_1	f_2	f_3
Wind LOF	0.43	0.80	0.62
Wind HAMF	0.44	0.60	0.33
Wave LOF	0.84	0.82	0.72
Wave HAMF	0.79	0.55	0.23

Table 4 Correlation coefficient (r_c) between the HAMF noise levels 2013 and wave height values at various distances (x in km) to the station.

x	r_c
50 - 100	0.74
250 - 300	0.83
450 - 500	0.86
650 - 700	0.77
850 - 900	0.73

Table 5 Spatial noise level variation of the vertical component of mainland stations for given time and frequency ranges ($f_1=0.125-0.25$ Hz; $f_2=0.5-5$ Hz; $f_3=2-10$ Hz). The numbers represent the average noise level of all stations minus the noise level of the individual ones in dB.

Station	January			July		
	f_1	f_2	f_3	f_1	f_2	f_3
\emptyset noise level	-121.82	-141.26	-146.39	-141.55	-142.95	-146.17
AKN	-4.18	1.04	2.06	0.89	0.55	-0.44
ARE0	0.95	5.25	10.14	2.27	4.81	5.39
ASK	1.81	0.81	1.94	-0.59	-1.01	2.41
BER	-0.11	-4.78	-10.64	2.32	-4.94	-9.40
BLS5	1.13	3.43	6.88	1.76	2.14	3.93
DOMB	-0.20	4.86	1.98	2.17	1.76	-2.28
HAMF	0.40	-3.48	-1.48	1.98	-1.52	-1.02
HOMB	5.12	-9.29	-15.92	-11.59	-8.23	-9.79
HYA	-0.25	-2.60	0.64	0.34	-1.61	2.07
KMY	1.26	-2.86	1.66	0.26	-4.07	-1.90
KONO	1.42	4.99	6.37	2.79	4.51	6.53
KONS	-3.59	-1.05	3.64	-13.37	-1.71	3.41
KTK1	0.93	2.84	4.51	-0.75	3.35	4.25
LOF	-0.41	-0.75	6.11	2.78	0.31	6.94
MOL	-0.48	-3.99	-9.49	0.99	-3.65	-8.90
MOR8	-1.43	3.79	5.46	1.71	3.55	4.91
NC602	-0.22	7.18	8.87	1.73	7.11	9.51
NSS	-1.83	2.32	4.40	-2.881	0.98	3.01
ODD1	1.13	2.58	2.47	-0.68	-1.95	-7.78
OSL	2.01	-3.67	-16.35	1.50	-4.33	-14.11
SKAR				3.40	5.58	6.19
SNART	-1.26	-0.31	-0.32	-3.27	1.10	0.41
STAV	1.81	-4.34	-9.88	1.39	-2.83	-5.53
STEI	-0.68	5.13	10.16	-0.34	4.37	9.83
SUE	-2.25	-2.59	2.71	3.23	-0.89	4.79
TBLU	-1.41	-4.81	-14.95	0.92	-5.17	-13.07
TRO	0.33	0.30	-0.97	1.04	1.79	0.63

Table 6 Spatial noise level variation of the vertical component of island stations for given time and frequency ranges ($f_1=0.125-0.25$ Hz; $f_2=0.5-5$ Hz; $f_3=2-10$ Hz). The numbers represent the average noise level of all stations minus the noise level of the individual station in dB.

Station	January			July		
	f_1	f_2	f_3	f_1	f_2	f_3
\emptyset noise level	-122.91	-133.15	-140.75	-139.52	-135.17	-141.78
BJO	-0.72	-5.64	-10.63	3.45	-2.81	-5.49
HOPEN	-0.31	-5.25	-9.01	-11.29	-12.49	-17.96
HSPB	8.18	5.95	5.11	2.53	5.68	6.85
JMIC	-10.93	-12.98	-18.00	-2.77	-5.92	-4.05
KBS	2.96	8.06	12.78	4.82	7.46	7.35
SPA0	0.83	9.87	19.74	3.26	8.07	13.30

Paper 2:
 Q_{Lg} wave tomography beneath Norway

Andrea Demuth, Lars Ottemöller and Henk Keers

Department of Earth Science,
University of Bergen, Allégaten 41, N-5007 Bergen, Norway

published in Journal of Seismology (2018)

Paper 3:
**Earthquake Source Parameters in Norway determined with Empirical
Green's functions**

Andrea Demuth, Norunn Tjøland and Lars Ottemöller

Department of Earth Science,
University of Bergen, Allégaten 41, N-5007 Bergen, Norway

submitted to Journal of Seismology

**Errata for
Ambient noise levels, Q_{Lg} wave tomography and
earthquake source parameters in Norway**

Andrea Demuth



Avhandling for graden philosophiae doctor (ph.d.)
ved Universitetet i Bergen

(sign kandidat)

(sign fakultet)



22.03.2019

Errata

Page i	blank page added before page ii
Page ii	blank page added before page iii
Page v	blank page added before page 1
Page 2	blank page added
Page 22	blank page added
Page 26	blank page added before paper manuscript
Page 47	blank pages added before and after page 47
Page 63	completed the text line submitted to 'Journal of Seismology'
Page 64	blank page added before paper manuscript
Page 76	blank page added

References

- Abercrombie, R. E., 1995. Earthquake source scaling relationships from -1 to 5 M_L using seismograms recorded at 2.5-km depth, *Journal of Geophysical Research*, **100**(B12), 24,015–24,036.
- Abercrombie, R. E., Bannister, S., Ristau, J., & Doser, D., 2017. Variability of earthquake stress drop in a subduction setting, the Hikurangi margin, New Zealand, *Geophysical Journal International*, **208**, 306–320.
- Aki, K., 1967. Scaling law of seismic spectrum, *Journal of Geophysical Research*, **72**(4), 1217–1231.
- Aki, K., 1980. Attenuation of shear-waves in the lithosphere for frequencies from 0.05 to 25 hz, *Physics of the Earth and Planetary Interiors*, **21**, 50–60.
- Ardhuin, F., Balanche, A., Stutzmann, E., & Obrebski, M., 2012. From seismic noise to ocean wave parameters: General methods and validation, *Journal of Geophysical Research*, **117**, C05002.
- Atakan, K., Lindholm, C. D., & Havskov, J., 1994. Earthquake swarm in Steigen, northern Norway: an unusual example of intraplate seismicity, *Terra Nova*, **6**, 180–194.
- Barmin, M. P., Ritzwoller, M. H., & Levshin, A. L., 2001. A fast and reliable method for surface wave tomography, *Pure and Applied Geophysics*, **158**, 1351–1375.
- Benz, H. M., Frankel, A., & Boore, D. M., 1997. Regional Lg attenuation for the continental United States, *Bulletin of the Seismological Society of America*, **87**(3), 606–619.
- Boatwright, J., 1980. A spectral theory for circular seismic source; simple estimates of source dimension, dynamics stress drop, and radiated seismic energy, *Bulletin of the Seismological Society of America*, **70**, 1–27.

- Brune, J. N., 1970. Tectonic stress and the spectra of seismic shear waves from earthquakes, *Journal of Geophysical Research*, **75**(26), 4997–5009.
- Bungum, H., Vaage, S., & Husebye, E. S., 1982. The Meløy earthquake sequence, northern Norway: source parameters and their scaling relations, *Bulletin of Seismological Society of America*, **72**(1), 197–206.
- Bungum, H., Olesen, O., Pascal, C., Gibbons, S., Lindholm, C., & Vestøl, O., 2010. To what extent is the present seismicity of Norway driven by post-glacial rebound?, *Journal of Geological Society*, **167**, 373–384.
- Campillo, M. & Plantet, J. L., 1991. Frequency dependence and spatial distribution of seismic attenuation in France: experimental results and possible interpretation, *Physics of the Earth and Planetary Interiors*, **67**, 48–64.
- D'Alessandro, A. & Ruppert, N., 2012. Evaluation of location performance and magnitude of completeness of the Alaska Regional Seismic Network by the SNES method, *Bull. Seismol. Soc. Am.*, **102**(5), 2098–2115.
- D'Alessandro, A., Luzio, D., D'Anna, G., & Mangano, G., 2011a. Seismic network evaluation through simulation: an application to the Italian National Seismic Network, *Bull. Seismol. Soc. Am.*, **101**(3), 1213–1232.
- D'Alessandro, A., Papanastassiou, D., & Baskoutas, I., 2011b. Hellenic unified seismological network: an evaluation of its performance through SNES method, *Geophysical Journal International*, **185**, 1417–1430.
- Díaz, J., Villasenor, A., Morales, J., Pazos, A., Cordoba, D., Pulgar, J., Garcia-Lobon, J., Harnafi, M., Carbonell, R., Gallart, J., & Group, T. S. W., 2010. Background Noise Characteristics at the IberArray Broadband Seismic Network, *Bull. Seismol. Soc. Am.*, **100**, 618–628.
- Erickson, D., McNamara, D. E., & Benz, H. M., 2004. Frequency-dependent L_g Q

- within the continental United States, *Bulletin of the Seismological Society of America*, **94**(5), 1630–1643.
- Eshelby, J. D., 1957. The determination of the elastic field of an ellipsoidal inclusion, and related problems, *Proceedings of the Royal Society of London*, **241**(1226), 376–396.
- Fan, G. & Lay, T., 2002. Characteristics of Lg attenuation in the Tibetan Plateau, *Journal of Geophysical Research*, **107**(B10), 2256.
- Gregersen, S., 1984. Crustal structure anomalies detected with Lg waves in grabens near continental margins in Greenland and the North Sea, *Marine Geophysical Researches*, **6**, 409–413.
- Hartzell, S. H., 1978. Earthquake aftershocks as Green’s functions, *Geophysical Research Letters*, **5**(1), 1–4.
- Hasegawa, H. S., 1983. Lg spectra of local earthquakes recorded by the east Canada Telemetered Network and spectral scaling, *Bulletin of the Seismological Society of America*, **73**(4), 1041–1061.
- Herrmann, R. B. & Kijko, A., 1983. Modeling some empirical vertical component Lg relations, *Bulletin of the Seismological Society of America*, **73**(1), 157–171.
- Hicks, E. C., Bungum, H., & Lindholm, C. D., 2000. Seismic activity, inferred crustal stresses and seismotectonics in the Rana region, northern Norway, *Quaternary Science Reviews*, **19**, 1423–1336.
- Ide, S., Beroza, G. C., Prejean, S. G., & Ellsworth, W. L., 2003. Apparent break in earthquake scaling due to path and site effects on deep borehole recordings, *Journal of Geophysical Research*, **108**(B5), 2271.
- Kanamori, H., 1977. The energy release in great earthquakes, *Journal of Geophysical Research*, **82**(20), 2981–2987.

- Kaneko, Y. & Shearer, P. M., 2014. Seismic source spectra and estimated stress drop derived from cohesive-zone models of circular subshear rupture, *Geophysical Journal International*, **197**, 1002–1015.
- Kennett, B. & Mykkeltveit, S., 1984. Guided wave propagation in laterally varying media - II. Lg-waves in north-western Europe, *Geophys. J. R. Astron. Soc.*, **79**, 257–267.
- Kvamme, L. B., Hansen, R. A., & Bungum, H., 1995. Seismic-source and wave-propagation effect of Lg waves in Scandinavia, *Geophysical Journal International*, **120**, 525–536.
- Malagnini, L., Mayeda, K., Nielsen, S., Yoo, S.-H., Mufafo, I., Rawles, C., & Boschi, E., 2014. Scaling transition in earthquake source: A possible link between seismic and laboratory measurements, *Pure and Applied Geophysics*, **171**, 2685–2707.
- Marzorati, S. & Bindi, D., 2006. Ambient noise levels in north central Italy, *Geochem. Geophys. Geosyst.*, **7**, Q09010.
- McNamara, D. & Buland, R., 2004. Ambient Noise Level in the Continental United States, *Bull. Seismol. Soc. Am.*, **94**, 1517–1527.
- McNamara, D. E. & Walter, W. R., 2001. Mapping crustal heterogeneity using Lg propagation efficiency throughout the Middle East, Mediterranean, Southern Europe and Northern Africa, *Pure and Applied Geophysics*, **158**, 1165–1188.
- Mori, J., Abercrombie, R. E., & Kanamori, H., 2003. Stress drops and radiated energies of aftershocks of the 1994 Northridge, California, earthquake, *Journal of Geophysical Research*, **108**(B11), 2545.
- Mueller, C. S., 1985. Source pulse enhancement by deconvolution of an empirical Green's function, *Geophysical Research Letters*, **12**(1), 33–36.

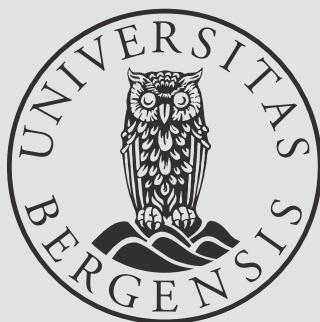
- Ottmöller, L., Shapiro, M., Singh, S. K., & Pacheco, J. F., 2002. Lateral variation of Lg wave propagation in southern Mexico, *Journal of Geophysical Research*, **107**(B1), ESE 3–1 ESE 3–13.
- Peterson, J., 1993. Observation and modeling of seismic background noise, *U.S. Geol. Surv. Tech. Rept.*, **93-322**, 1–95.
- Pirli, M., Schweitzer, J., Ottmöller, L., Raeesi, M., Mjelde, R., Atakan, K., Guterch, A., Gibbons, S. J., Paulsen, B., Debski, W., Wiejacz, P., & Kværna, T., 2010. Preliminary analysis of the 21 February 2008 Svalbard (Norway) seismic sequence, *Seismological Research Letters*, **81**(1), 63–75.
- Prieto, G. A., Shearer, P. M., Vernon, F. L., & Kilb, D., 2004. Earthquake source scaling and self-similarity estimation from stacking p and s spectra, *Journal of Geophysical Research*, **109**, B08 310.
- Rastin, S., Unsworth, C., Gledhill, K., & McNamara, D., 2012. A Detailed Noise Characterization and Sensor Evaluation of the North Island of New Zealand Using the PQLX Data Quality Control System, *Bull. Seismol. Soc. Am.*, **102**, 98–113.
- Sereno, T. J., Bratt, S. R., & Bache, T. C., 1988. Simultaneous inversion of regional wave spectra for attenuation and seismic moment in Scandinavia, *Journal of Geophysical Research*, **93**(B3), 2019–2035.
- Shapiro, N., Béthoux, N., Campillo, M., & Paul, A., 1996. Regional seismic phases across the Ligurian Sea: Lg blockage and oceanic propagation, *Physics of the Earth and Planetary Interiors*.
- Shi, J., Kim, W.-Y., & Richards, P. G., 1998. The corner frequencies and stress drops of intraplate earthquakes in the northeastern United States, *Bulletin of the Seismological Society of America*, **88**(2), 531–542.
- Singh, S. & Herrmann, R. B., 1983. Regionalization of crustal coda Q in the continental United States, *Journal of Geophysical Research*, **88**(B1), 527–538.

Viegas, G., Abercrombie, R. E., & Kim, W.-Y., 2010. The 2002 M5 Au Sable Forks, NY, earthquake sequence: Source scaling relationships and energy budget, *Journal of Geophysical Research*, **115**, B07 310.

Zhang, T. R. & Lay, T., 1995. Why Lg phase does not traverse oceanic crust, *Bulletin of the Seismological Society of America*, **85**, 1665–1678.



Graphic design: Communication Division, UIB / Print: Skjipes Kommunikasjon AS



uib.no

ISBN: 978-82-308-3515-9